Dissolved oxygen and triple oxygen isotope measurements provide different insights into gross oxygen production in a shallow salt marsh pond

Evan M. Howard, Amanda C. Spivak, Jennifer S. Karolewski, Kelsey M. Gosselin, Zoe O. Sandwith, Cara C. Manning, and Rachel H. R. Stanley

This is a post-peer-review, pre-copyedit version of an article published in *Estuaries and Coasts*. The final authenticated version is available online at: https://doi.org/10.1007/s12237-020-00757-6.

The electronic supplementary material are freely available through the link above.

Please cite the published article:

Howard, E.M., Spivak, A.C., Karolewski, J.S., Gosselin, K.M, Sandwith, Z.O, Manning, C.C., and Stanley, R.H.R. Oxygen and Triple Oxygen Isotope Measurements Provide Different Insights into Gross Oxygen Production in a Shallow Salt Marsh Pond. *Estuaries and Coasts* 43**,** 1908–1922 (2020). https://doi.org/10.1007/s12237-020-00757-6

Title:

Dissolved oxygen and triple oxygen isotope measurements provide different insights into gross oxygen production in a shallow salt marsh pond

Authors and affiliations:

Evan M. Howard[1], Amanda C. Spivak[2], Jennifer S. Karolewski[3], Kelsey M. Gosselin[4], Zoe O. Sandwith[5], Cara C. Manning[6], Rachel H. R. Stanley[7]

[1] School of Oceanography, University of Washington, Seattle, WA, USA. Orcid: 0000-0002-1993-0692

[2] Department of Marine Sciences, University of Georgia, Athens, GA, USA. Orcid: 0000-0001-6743-0783.

[3] MIT-WHOI Joint Program in Oceanography, Cambridge and Woods Hole, MA, USA. Orcid: NA

[4] Department of Earth Science, University of California Santa Barbara, Santa Barbara, CA, USA. Orcid: 0000-0002-9327-8954

[5] Department of Marine Chemistry and Geochemistry, Woods Hole Oceanographic Institution, Woods Hole, MA, USA. Orcid: 0000-0001-9952-9526

[6] Department of Earth, Ocean and Atmospheric Sciences, University of British Columbia, Vancouver, BC, Canada. Orcid: 0000-0002-4984-5093

[7] Department of Chemistry, Wellesley College, Wellesley, MA, USA. Orcid: 0000-0003-4860-2476

Abstract

The metabolism of estuarine environments is often estimated by measuring changes in dissolved oxygen concentrations. A central assumption of common oxygen-based approaches is that oxygen consumption rates (primarily respiration) are similar under light and dark conditions. Evaluating this assumption is critical, especially in benthic-dominated systems, because differences between daytime and nighttime respiration could result in underestimation or overestimation of ecosystem productivity. We evaluated rates of gross oxygen production over hourly to seasonal time scales in a shallow, temperate salt marsh pond. To assess whether a dissolved oxygen diel mass balance underestimated gross oxygen productivity, we compared rates using this traditional approach and using the triple oxygen isotope tracer of photosynthesis. This is a powerful combination because the triple oxygen isotope approach is theoretically insensitive to respiration. The methods agreed well over daily to seasonal time scales. However, during midday periods of peak light and productivity, the triple oxygen isotope approach resulted in higher hourly-scale gross oxygen production rates. The timing and magnitude of this short-term difference is consistent with light-dependent oxygen uptake fluxes including photoreduction and/or light-stimulated community respiration. Finally, aquatic vegetation was associated with variability in productivity across the pond. Such small scale environmental heterogeneity is evidence that this shallow pond was not laterally well mixed, and likely contributes to the dynamism of these common estuarine environments.

Keywords (4-6)

metabolism, light-dependent respiration, oxygen , triple oxygen isotopes, salt marsh, pond

1. Introduction

Dissolved oxygen (O_2) fluxes are widely used to estimate aquatic ecosystem metabolism rates, including in lakes (Staehr et al. 2010), streams (Demars et al. 2015), estuaries (Caffrey 2004), and the ocean (Yang et al. 2017). However, attribution of these fluxes to photosynthesis and respiration is complicated because the physical and biological processes that affect net oxygen fluxes vary over time and space and may be difficult to disentangle without additional tracers. In particular, deriving photosynthesis rates from a dissolved O_2 mass balance typically requires either assuming that nighttime respiration is representative of daytime respiration (e.g. Odum 1956, Staehr et al. 2010) or using submodels of photosynthesis as a function of irradiance and respiration as a function of temperature (Holtgrieve et al. 2010, Winslow et al. 2016). Neither approach accounts for light-dependent increases in ecosystem respiration or non-respiratory O_2 uptake. Yet, O_2 consumption in aquatic ecosystems including sediments and pelagic environments in lakes, estuaries, and the open ocean may be two to ten times greater in the light than in the dark (Falkowski and Owens 1978, Bender et al. 1987, Kana 1990, Epping and Jørgensen 1996, Parkhill and Gulliver 1998, Pringault et al. 2009). The same studies found that if light-dependent O_2 uptake is not explicitly accounted for, photosynthetic production may be underestimated by 23 – 62%.

Thus ecosystem rates of photosynthesis and respiration based on dissolved O_2 fluxes may be systematically too low, complicating assessment of O_2-driven biogeochemistry and attribution of changes in ecosystem metabolism rates to environmental drivers.

Observations of light-dependent O_2 consumption are generally derived from concurrent comparisons between net O_2 fluxes and either production or respiration, separately evaluated using other methods. Some studies measure either short-term responses to light, including

67 methods based on fluorometry (Suggett et al. 2009) and hysteresis of dissolved O_2 responses to
68 irradiance changes (Falkowski and Owens 1978, Epping and Jørgensen 1996). Others compare
69 net O_2 or carbon fluxes to photosynthetic production evaluated with carbon or oxygen isotope
70 labeling of photosynthetic substrates (Bender et al. 1987, Laws et al. 2000). Laboratory studies
71 may inhibit specific cellular pathways in order to isolate the particular light-dependent O_2
72 process of interest (e.g. Helman et al. 2005). Each method has different sensitivities to different
73 mechanisms of O_2 uptake. This diversity of tracers and methods used can complicate the
74 attribution of measured O_2 fluxes to specific light-dependent processes as opposed to
75 methodological biases. It is therefore challenging to generalize the wide range of light-dependent
76 effects on respiration and productivity reported in the literature.

77 One promising approach for estimating *in situ* photosynthesis in aquatic environments is the
78 triple oxygen isotope (TOI) method (Luz and Barkan 2000), which involves the simultaneous
79 measurement of natural abundance ^{16}O, ^{17}O, and ^{18}O of O_2 dissolved in water. The oxygen
80 isotope ratios can be combined in a respiration-independent manner in order to calculate the
81 fraction of dissolved O_2 derived from splitting of water in photosystem II during photosynthesis
82 compared to the fraction of O_2 entering the water through air-water gas exchange. Thus the
83 evolution of the oxygen isotope ratios with time provides an unambiguous estimate of gross
84 oxygen production (GOP), similar to the $H_2{}^{18}O$ isotopic spike method (Bender et al. 1987).
85 However, a crucial difference between the TOI method and $H_2{}^{18}O$ or other incubation methods is
86 that the natural abundance triple oxygen isotopes can be used to evaluate photosynthesis *in situ*,
87 in intact ecosystems, whereas incubation methods require removing organisms from their natural
88 system (e.g. into bottles). Used in this way, the TOI method for estimating GOP shares a major
89 source of systematic uncertainty with the dissolved O_2-derived production: air-water gas

exchange. This facilitates a direct comparison with dissolved O_2 fluxes derived from *in situ* sensors in a common O_2 "currency," and allows evaluation of O_2 uptake in the light under ambient environmental conditions. The shared uncertainties and sensitivity to *in situ* conditions of these two methods contrasts with the primarily incubation-based approaches outlined above, in which results may diverge from whole ecosystem production and respiration rates because of altered growth environments ("bottle effects") or subsampling of the heterogeneous autotrophic and heterotrophic community of organisms.

Differences between TOI and dissolved O_2-derived rates of gross O_2 production should directly reflect the importance of light-dependent O_2 uptake processes (section *2.1.3*). Yet despite this potential utility and increasing adoption of this approach (e.g. Juranek and Quay 2013), the TOI method has rarely been directly compared to GOP from dissolved O_2 fluxes. Sarma et al. (2005) reported GOP from *in situ* TOI measurements to be nearly twice that derived from O_2 in light-dark bottle incubations for the surface mixed-layer of a coastal setting, though that ratio varied seasonally. In a Lagrangian study in the surface mixed-layer of the pelagic ocean, Hamme et al. (2012) found that *in situ* GOP rates from the TOI method ranged from half to double the GOP from an O_2 diel mass balance, though the two rates were not significantly different after a sufficiently long period elapsed. In a shallow estuary, Stanley and Howard (2013) found that the GOP derived from either method agreed when both the oxygen isotopes and dissolved O_2 were measured in benthic chambers at hourly frequencies. To the best of our knowledge, no previously published work has compared *in situ* GOP fluxes from the two methods across the range of time scales (hourly to seasonal) that O_2 data are commonly collected for studies of freshwater and estuarine metabolism.

112 In this work, we compare *in situ* photosynthetic rates derived from a standard dissolved O_2 diel
113 mass balance to those from the TOI method in a salt marsh pond. These shallow, continuously
114 submerged environments are well-lit, highly productive, have high rates of aerobic and anaerobic
115 sedimentary respiration producing reduced compounds, and undergo large diel changes in O_2
116 concentrations (Spivak et al. 2017, 2018). These characteristics have been identified as likely to
117 stimulate light-dependent O_2 uptake in other environments (Falkowski and Raven 1997, Fenchel
118 and Glud 2000, Buapet et al. 2013). Because we apply both the TOI and dissolved O_2 mass
119 balance methods to *in situ* data collected at the same time from the same salt marsh pond,
120 sources of systematic error between approaches are limited and incubation effects are eliminated;
121 any differences in O_2 production rates between the two approaches are more confidently
122 assigned to light-dependent O_2 uptake. Our goals are to: 1) evaluate whether GOP rates from the
123 TOI and dissolved O_2 diel mass balance are in good agreement or show systematic biases over
124 seasonal, daily, or hourly time scales; 2) determine the magnitude and significance of light-
125 dependent O_2 uptake in this setting; and 3) discuss the relationship of TOI and dissolved O_2
126 derived ecosystem metabolism fluxes to variations in environmental properties.

127

128 ## 2. Methods

129 ### *2.1 Theory*

130 #### *2.1.1 Dissolved O_2 diel method*

131 The dissolved oxygen mass balance for a parcel of water depends on production, respiration, air-
132 water gas exchange, light-dependent processes that consume O_2, entrainment and mixing with
133 adjacent water parcels, and bubble processes including wave driven bubble injection and partial

bubble exchange, and ebullition from underlying sediments. We do not quantify mixing or bubble processes, as neither could be adequately constrained over the entire study period, but consider the effects of these processes in the discussion. The resulting simplified O_2 mass balance for a well-mixed water parcel is expressed as:

$$h\frac{\partial}{\partial t}([O_2]) = GOP_{O2} - R + k_{O2}([O_2]_{sat} - [O_2]) - LD \quad (1)$$

Here h is the depth of the well-mixed water parcel being considered, $[O_2]$ and $[O_2]_{sat}$ are the measured and air-water saturation (at equilibrium) concentrations of dissolved O_2, GOP_{O2} is the areal gross oxygen production rate, R is the areal community respiration rate, k_{O2} is the air-water gas transfer velocity, and LD is the areal rate of a light-dependent process that results in net consumption of O_2. k_{O2} is calculated from wind speed and pond area using the parameterization of Vachon and Prairie (2013).

Only the sum of the oxygen producing and consuming processes can be directly evaluated from dissolved O_2 data. If light-dependent processes are minor contributors then the net biological O_2 flux is equivalent to net ecosystem metabolism ($NEM = GOP_{O2} - R$, sometimes alternatively referred to as net community production). In order to calculate GOP_{O2}, R is assumed to equal net oxygen uptake measured during nighttime periods (GOP_{O2} and PD equal zero), and assumed to be identical in the day (Odum 1956). We use this simple approach and note that it yields similar results to more nuanced calculations (Spivak et al. 2017) informed by temperature dependence of respiration and production (Yvon-Durocher et al. 2012) and light-dependent parameterizations of photosynthesis (Winslow et al. 2016). To the degree this assumption is incorrect GOP_{O2} and GOP derived from the triple oxygen isotopes, GOP_{TOI}, would diverge in a manner which provides additional information about environmental drivers of respiration.

2.1.2 Triple oxygen isotope method

Ratios of the three stable oxygen isotope ratios ($^{18}O/^{17}O/^{16}O$) can be used to define the TOI tracer $^{17}\Delta$ (defined after Angert et al. 2003):

(2) $$^{17}\Delta = \left[\ln\left(^{17}X\right) - \lambda \ln\left(^{18}X\right)\right] \times 10^{6} \text{ per meg}$$

^{i}X relates the isotopic ratio of dissolved oxygen (*i* denotes the heavier isotope) to that in the atmospheric air standard, e.g. $^{i}X = (^{i}O/^{16}O)_{sample}/(^{i}O/^{16}O)_{air}$. Per meg notation is used to denote part per million level variation in gas ratios (Keeling et al. 1998). λ is the ratio of the mass dependent isotope enrichment factors for $^{17}O/^{16}O$ and $^{18}O/^{16}O$. λ is constant within uncertainties for mitochondrial respiration (and photorespiration via RuBisCo) in the photosynthesizers cultured and measured to date (λ =0.518; Helman et al. 2005, Luz and Barkan 2005, Eisenstadt et al. 2010); thus $^{17}\Delta$ is defined to be respiration independent with λ. We use this conventional value to represent the pond community, however recent work suggests that a higher value (λ =0.522) is better supported by theory and recent dark respiration experiments in a freshwater reservoir (Ash et al. 2020); substituting this higher value results in qualitatively similar results in this work, and does not alter our conclusions (Online Resource S2).

Photosynthetic O_2 has a high value of $^{17}\Delta$ similar to the isotopic composition of the water from which it is derived (Luz and Barkan 2000), while atmospheric oxygen has low $^{17}\Delta$ resulting from mass independent fractionation of ozone in the stratosphere (Thiemens 2001). Therefore greater values of $^{17}\Delta$ in dissolved O_2 indicate increased photosynthetic production relative to gas exchange with the atmosphere.

Gross primary production independent of normal, mitochondrial respiration can then be calculated from an isotopic mass balance of dissolved oxygen (Kaiser 2011, Prokopenko et al.

2011). We provide full derivations and equations for the triple oxygen isotopic mass balance in **Online Resource S1**, including mixing and bubble processes not quantified in this work. The resulting abbreviated isotopic mass balance in terms of the measured isotopic ratios and $^{17}\Delta$ can be written as:

(3a) $h[O_2]\frac{\partial}{\partial t}\left(^{17}\Delta\right)$ *Change in tracer with time*

(3b) $= \mathrm{GOP_{TOI}}\left(\frac{^{17}X_w\,^{17}\alpha_p - ^{17}X}{^{17}X} - \lambda\frac{^{18}X_w\,^{18}\alpha_p - ^{18}X}{^{18}X}\right)$ *Gross oxygen production*

(3c) $+ k_{O2}[O_2]_{sat}\left(\frac{^{17}X_a\,^{17}\alpha_e\,^{17}\alpha_k - ^{17}X}{^{17}X} - \lambda\frac{^{18}X_w\,^{18}\alpha_e\,^{18}\alpha_k - ^{18}X}{^{18}X}\right)$ *Air-water gas exchange*

$$- k_{O2}[O_2]\left(\left(^{17}\alpha_k - 1\right) - \lambda\left(^{18}\alpha_k - 1\right)\right)$$

(3d) $- \mathrm{LD}\left(\left(^{17}\alpha_{ld} - 1\right) - \lambda\left(^{18}\alpha_{ld} - 1\right)\right)$ *Light-dependent process*

X_a and X_w refer to the isotopic endmembers for air (1 when air is the reference) and water (calculated as a mixture of seawater and meteoric water; Manning et al. 2017). X without a subscript refers to the measured ratios of dissolved O_2. α represents the isotopic fractionation factors associated with production (α_p, kinetic; Eisenstadt et al. 2010, Luz and Barkan 2011), air-water gas exchange (α_e, equilibrium; Benson and Krause 1980, 1984, Reuer et al. 2007; α_k, kinetic; Li et al. 2019), and the light-dependent process of interest (α_{pd}, kinetic; Helman et al. 2005)—Equation 3d assumes that the light-dependent process removes O_2 isotopically similar to that in the surrounding water rather than directly consuming O_2 from photosystem II (Kana 1990, Bender et al. 1999). Constants are chosen or calculated based on the preceding references (and summarized in **Online Resource S1**), however other choices may be appropriate for alternative definitions of $^{17}\Delta$ (Kaiser 2011, Nicholson 2011, Kaiser and Abe 2012). The rate of bulk O_2

198 change is explicitly included in the derivation of Equation 3 (Kaiser 2011, Prokopenko 2011).
199 **Online Resource S1** includes an example calculation. The Matlab toolbox 'calcGOP' also may
200 be used to calculate resulting GOP_{TOI} using Equations 3a-c (with the simplifying assumptions
201 that α_k=1 and α_p is the average value for marine phytoplankton; Manning and Howard, 2017).

202 *2.1.3 Light-dependent oxygen uptake processes*

203 Light-dependent O_2 consumption is variously attributed to five major processes: photoreduction
204 (Falkowski and Raven 1997), photorespiration (Buapet et al. 2013), light-stimulation of
205 mitochondrial ("dark") respiration in autotrophs (Grande et al. 1989), indirect stimulation of
206 heterotroph respiration via release of labile dissolved organic carbon by photosynthesizers (Laws
207 et al. 2000, Pringault et al. 2009), and, in benthic environments, oxidation of reduced compounds
208 stored in sediments (Fenchel and Glud, 2000). Each of these processes are expected to lead to
209 larger GOP_{TOI} than GOP_{O2}: Photoreduction can cause higher GOP_{TOI} but does not affect GOP_{O2},
210 while the other processes all decrease GOP_{O2} but are not expected to significantly affect GOP_{TOI}.
211 These effects are summarized in **Table 1**, and described further in **Online Resource S2**.

212 *2.2 Data collection and analysis*

213 *2.2.1 Setting*

214 The study site was a salt marsh pond, located at the Plum Island Ecosystems Long Term
215 Ecological Research site in Massachusetts, USA (42.7411° N, 70.8309° W). The pond was
216 approximately 7000 m^2 in area with a 25 cm mean depth. The pond was situated in the high
217 marsh, which is predominantly vegetated by *Spartina patens*, and proximal to a tidal creek. The
218 pond flooded with water from the surrounding tidal creek during the highest spring-tides,
219 roughly once daily over a few successive days every two weeks. Ecosystem metabolism and

environmental heterogeneity (Spivak et al. 2017, 2018), diel cycling of microbial processes (Kearns et al. 2018), and air-water gas exchange and ebullition (Howard et al. 2018) have been previously examined in this pond.

2.2.2 Sampling methods

Temperature, electrical conductivity (and resulting salinity), and O_2 saturation data were collected at 15 min frequency, from May 7 to October 28, 2014. Sensor data were recorded at a single location over sediment without macrophytes, far from the pond banks (**Fig. 1**). Sensors were deployed approximately 10 cm above the sediment-water interface. The sensors were cleaned and calibrated (pre- and post-deployment) approximately every two weeks. Calibrations included one-point O_2 calibration to water-saturated air (with initial zero-O_2 calibration in May 2014), and two-point conductivity calibrations (1×10^4 and 5×10^4 µS cm^{-1} YSI™ standards). Additional details of sensor deployment, cross-calibration, and *post hoc* correction of salinity are in the supporting information (**Online Resource S2**)—no sensor drift or offsets between different sensor deployments were observed for temperature and O_2.

Photosynthetically active radiation flux (PAR, 400-700 nm wavelengths) and meteorological data used to calculate air-water gas exchange were collected at a meteorological tower 200 m northeast from the study site (Forbrich and Giblin 2015). Air-water gas exchange was calculated from meteorological data as described in Howard et al. (2018) using the wind speed based parameterization of Vachon and Prarie (2013). *In situ* and air-water equilibrium concentrations of O_2, $[O_2]$ and $[O_2]_{eq}$ (Garcia and Gordon 1992, 1993), were smoothed using a 30 minute (n=3) moving mean to limit instrument signal noise.

241 Samples for TOI analysis were collected approximately weekly, during 20 daytime periods when
242 the pond was tidally isolated from the adjacent tidal creek. Pond water was collected in pre-
243 poisoned, 500 mL evacuated glass flasks, which were filled with roughly 300 mL of water while
244 submerged at 10 cm depth. Care was taken to exclude bubbles and debris, and samples were
245 collected 2 m from the pond edge using an inner-tube to avoid suspending sediments during
246 sampling. Samples were collected over bare sediments at three or more timepoints between
247 10:00 and 14:00, with a few days including early morning and evening periods. Additionally,
248 concurrent time series over macroalgae (*Ulva intestinalis*) or rooted vascular plants (*Ruppia*
249 *maritima*) were collected on several days. In order to evaluate replicate uncertainty in the TOI
250 samples, two to five replicate samples were collected at 19 different times over the course of the
251 study.

252 Additional O_2 saturation state, temperature, and salinity data were collected simultaneously with
253 each TOI bottle sample using a handheld YSI^{TM} Pro-ODO sensor (accuracy and precision 0.1+/-
254 0.2 °C and 2±0.2 % of oxygen saturation) and handheld refractometer (2+/-1 on PSS-78). Both
255 instruments were calibrated daily. Along the western edge of the pond where most daily time
256 series were conducted, these measurements were similar to conditions at the sensor location.
257 However, conditions were more varied around the pond perimeter, particularly on the eastern
258 side of the pond where submerged grasses and macroalgae were more abundant. O_2 saturation
259 state and temperature were surveyed in the morning and midday on May 29th, July 17th, July 23rd,
260 August 7th, September 23rd, and October 13th.

261 Total sediment cover of submerged *Ruppia* and *Ulva* was visually estimated over 11 weeks
262 between June 25th and August 13th as well as between November 11th and November 25th
263 (Spivak et al. 2017). On each occasion, macrophyte cover was assessed from three 1 m^2 quadrats

randomly sampled along each of two crossing transects (different transects for each sample period) for a total of six sample locations. All percent cover data were pooled to map the average conditions over the sampling season, and binned and averaged over a 5 m by 5 m grid. To fill missing data, we used an image interpolation and extrapolation approach (Matlab function 'inpaint_nans,' method 4; D'Errico 2012). This method generates equivalent results to linear interpolation, but behaves conservatively during spatial extrapolation to fill missing data within the limits of (no higher than) adjacent sampled data (**Online Resource S2**).

2.2.3 Triple oxygen isotope analysis

Water and gas headspace in the TOI samples were equilibrated at room temperature and the headspace was processed on an automated cryogenic line which collected O_2 and Argon (Ar) while separating and discarding water vapor and dinitrogen gas (Stanley and Howard 2013). Oxygen isotope ratios were measured on a Thermo Scientific MAT 253 isotope ratio mass spectrometer. Every sample was compared to a gas secondary standard with similar O_2/Ar to seawater (Scott Specialty Gases); sample and standard voltages were balanced, resulting in similar pressure within the mass spectrometer. Samples were additionally referenced to both a gas primary standard (atmospheric air from Woods Hole, MA, USA) and air-equilibrated de-ionized water (blank solutions with no biological signature), which were run every nine samples. Samples were corrected for ion source interactions with Ar (Abe and Yoshida 2003) when O_2/Ar ratios were sufficiently high that Ar matrix corrections were less than roughly 10% of the magnitude of measured isotope ratios, which was generally true at >70% of O_2 saturation. At lower O_2/Ar ratios (e.g. early morning samples), Ar and any trace methane was additionally stripped from the gas sample prior to measurement (**Online Resource S2**). Using either method, the oxygen isotope ratios were additionally corrected for sample size (Stanley et al. 2010), and

small differences between $^{17}\Delta$ calculated from calibrated $^{18}O/^{16}O$ and $^{17}O/^{16}O$ versus those on $^{17}\Delta$ directly (Howard et al. 2017) in order to determine precise isotope ratios over the entire range of O_2 concentrations in the pond. Each calibration was well-described as a linear function of isotopic composition (a few percent relative error in the slopes). There was no indication that pressure baseline errors were an important source of uncertainty following calibrations, in either the O_2/Ar or pure O_2 samples (**Online Resource S2**).

Water standards run concurrently with our samples were precise to 3 $x10^{-2}$ per mil in $^{17}O/^{16}O$, 5 $x10^{-2}$ per mil in $^{18}O/^{16}O$, and 6 per meg in $^{17}\Delta$ (6 $x10^{-3}$ per mil; standard deviations for n=51 water standards). Sample replicate precision was 7 $x10^{-2}$ per mil in $^{17}O/^{16}O$, 13 $x10^{-2}$ per mil in $^{18}O/^{16}O$, and 5 per meg in $^{17}\Delta$ (4% relative error in all three measures). Water standards were not significantly different using either the high or low O_2/Ar ratio methods ($p>0.9$ for Welch's t-test with null hypothesis of different population means for all isotopic variables).

2.2.4 Ecosystem metabolism rate calculations

Equations 1 and 3 were discretized and rearranged to determine particular rates of interest. Changes over the period spanning two sampled times were calculated using midpoint values of the continuous variables (e.g. concentrations, air-water gas transfer velocity, isotopic ratios). For direct comparison of hourly GOP_{TOI} and GOP_{O2}, GOP_{O2} was averaged over a 90 minute window centered on the time of GOP_{TOI}, similar to the TOI sampling frequency.

In order to compare full day rates of GOP_{TOI} and GOP_{O2}, integrated GOP_{TOI} during the midday observational period was multiplied by the ratio of the integrated dawn-dusk PAR over the integrated PAR during the TOI sampling period. We took this simple scaling approach because a single photosynthesis-irradiance (P-I) curve could not fit all the GOP results over the six month

time series, and there were generally insufficient data to fit daily P-I curves. However, unsampled periods were generally at low PAR, where GOP and PAR should have been linearly related. Indeed, even without excluding samples from periods likely beyond the saturating irradiance, integrated GOP_{TOI} and PAR over each hour-scale measurement period were significantly linearly correlated (r=0.53, p=3×10^{-7} for a null hypothesis of no correlation, 35% uncertainty in correlation slope). Further, the unsampled morning and evening periods generally contributed less than a quarter of integrated PAR. Thus the theoretical errors associated with this approach (≤20%, relative standard deviation) were of similar size to other uncertainties. For the three daily time series in which TOI was sampled in mornings and evenings, daily GOP_{TOI} agreed well with the PAR-scaled daily GOP_{TOI} derived from the 10:00-14:00 samples—the ratio of measured to scaled GOP_{TOI} was 1.0(0.1; standard deviation; no bias between rates).

Both hourly and daily average rates are reported in terms of areal production per hour, for comparability of the magnitude and variability of rates over different time scales.

2.2.5 Statistics

In order to examine environmental variability, the effect of the variability of O_2 changes was calculated by taking the standard deviation of all measured rates of change at each sample location over the study and dividing by the average of standard deviations at all sample locations. This normalized effect size highlights where in the pond temporal variability in oxygen changes is highest or lowest—e.g. an effect size of 2 means that on average, O_2 saturation state at a location increased twice as much as the mean across the pond.

GOP, R, and NEM errors were propagated from each input variable's standard probability distribution via a Monte Carlo simulation with 10,000 iterations, with the standard deviation

331 across all iterations reported as the rates' uncertainties. Shared sources of systematic uncertainty
332 between both TOI and dissolved O_2 derived metabolic rates were not included in uncertainty
333 estimates (e.g., uncertainties in the parameterizations of the gas transfer velocity and O_2
334 solubility), but random errors expected to vary between sample locations and times were
335 included (e.g., short-term variability in wind, instrumental precision of measured O_2 saturation
336 state, and changes in solubility driven by temperature heterogeneity within the pond).
337 Uncertainties for subsequent comparisons of metabolic rates were calculated in quadrature.

338 In order to determine whether short, daily to weekly changes of environmental parameters in
339 time contributed to changes in daily GOP_{O2} and R, the time series of each environmental
340 property considered (temperature, PAR, windspeed, wind direction, and tidal flooding) were
341 detrended to remove autocorrelation (prewhitened) using an Autoregressive Integrated Moving
342 Average (ARIMA) procedure with the 'arima.m' function in Matlab. Differencing,
343 autoregressive (lag), and moving average (smoothing) terms were assigned based on analysis of
344 the autocorrelation and partial autocorrelation functions of for the variables of interest, with the
345 goal of reducing the residuals of the observations versus the ARIMA model to white noise. An
346 additional periodic term was used in the tidal stage ARIMA. The cross-correlation coefficients
347 (r) between the residuals of the environmental variable and metabolic rates relative to the
348 ARIMA model for that environmental variable were then calculated.

349 Correlations of GOP_{TOI} with environmental variables were calculated based on only the subset of
350 data from days when GOP_{TOI} was sampled. Data were not prewhitened for any variables in this
351 reduced subset because of the small number of samples and discontinuous time series—
352 autocorrelations and partial-autocorrelations were already near-zero and not reduced by an
353 ARIMA procedure.

Throughout, p values are presented for the following statistical tests, unless otherwise specified: Significance of linear correlations are evaluated for the null hypotheses of no correlation or a regression differing in sign (a one-tailed distribution), using Fisher's z-transformation on the linear correlation coefficients, r, and evaluating resulting tails of the normal cumulative distribution functions. Alternatively, significance of bias (mean rate difference of one method relative to the other) is evaluated with the null hypothesis of zero difference using a paired sample Student's t-test. Standard deviations or relative standard deviations are noted in parentheses following mean values (e.g. mean(standard deviation)). Linear correlations use Model II regressions, in which root mean square errors are calculated normal to the regression slope (neither variable is assumed to be independent and error free); r are reported for the linearity of regressions, and, where data is normally distributed, r^2 is used to calculate the fraction of total variance shared by regressed variables.

3. Results

3.1 Metabolic rate comparison

On hourly time scales, GOP_{O2} and GOP_{TOI} (**Fig. 2a-c**) were significantly correlated (r=0.45, p=1×10^{-5}). Both GOP rates generally peaked concurrently with daily PAR (Figure S1 in **Online Resource S2**). However, the magnitude of hourly GOP_{TOI} tracked hourly fluctuations in PAR more closely than GOP_{O2} did (**Fig. 2a-c**). This resulted in greater divergence between methods (GOP_{TOI}-GOP_{O2}) with larger changes in PAR within a day (r=0.24, p=4×10^{-2}; correlation of z scores standardized by day). In part because of this differing sensitivity, the two GOP rates exhibited coarse agreement overall (**Fig. 3a**; limits of agreement—95% confidence intervals

surrounding the mean rate difference—were 15 mmol O_2 m^{-2} h^{-1}, similar to peak midday rates), and GOP_{TOI} was on average slightly greater than GOP_{O2} (GOP_{TOI}-GOP_{O2}=1.6 mmol O_2 m^{-2} h^{-1}, p=0.05). This mean difference (bias) was not significant when normalized to the magnitude of production (**Fig. 3b**; [GOP_{TOI}-GOP_{O2}]/mean[GOP_{TOI}, GOP_{O2}]=0.1, $p=3\times10^{-1}$). Despite the lack of major biases in the mean, the rate differences were correlated to the magnitude of GOP in both absolute (r=0.35, $p=1\times10^{-3}$) and relative terms (r=0.23, $p=4\times10^{-2}$).

Hourly NEM was autotrophic at midday, but heterotrophic in the morning and evening. Overnight R was relatively constant despite hourly variability, and of similar magnitude to daytime GOP.

Daily rates of GOP_{O2} and GOP_{TOI} (scaled to PAR, section *2.2.4*; **Fig. 2d**) were similarly significantly correlated (r=0.56, $p=1\times10^{-2}$) and in broad agreement (**Fig. 3c**, **d**; limits of agreement were 6 mmol O_2 m^{-2} h^{-1}). There was no significant bias between rates (absolute difference: 0.2 mmol O_2 m^{-2} h^{-1}, $p=8\times10^{-1}$; relative difference: 0.0, $p=7\times10^{-1}$) or rate divergence as a function of production (correlation of absolute rate difference to mean GOP: r=0.38, $p=1\times10^{-1}$; correlation of relative difference: r=0.41, $p=8\times10^{-2}$). Both GOP_{TOI} and GOP_{O2} followed similar seasonal patterns, with generally increasing rates in May through August and lower rates in mid-September through October.

Daily respiration rates similarly decreased from summer into fall, while daily NEM was relatively constant and heterotrophic over the time series. Large, synchronous decreases in GOP_{O2}, NEM, and R lasting several days were associated with periods of spring tide flooding of the pond. It is unclear whether these rate decreases reflect homogenization of metabolic tracers across the marsh environment during periods of tidal interconnectivity or limitations of the mass

balance in the presence of potential lateral fluxes; in either case GOP_{TOI} was not evaluated during periods of tidal flooding.

3.2 Spatial environmental heterogeneity

Temperature, O_2 saturation state, the TOI ratios ($^{17}\Delta$), and GOP_{TOI} varied across the pond (Table S1 in **Online Resource S3**), particularly along the eastern edge where plant and macroalgal abundance was high. The southernmost portion of the pond also had macroalgal cover (e.g. sample location 4, **Fig. 1**), but was omitted from weekly surveys to minimize interference with concurrent experiments. The spatial surveys on May 29 were broadly representative of variability observed across the time series (**Fig. 4**): In the morning, temperature, O_2 saturation state, and $^{17}\Delta$ were similar around the pond. However, by midday the areas with more vegetation were generally warmer and had higher O_2 saturation state and $^{17}\Delta$. The same areas had greater and more variable rates of dissolved O_2 increases across the time series (**Fig. 5**, Table S2 in **Online Resource S3**). Compared to unvegetated areas, these observations were consistent with increased accumulation of photosynthetic O_2 relative to gas exchange with the atmosphere (**Fig. 4**), but not necessarily higher production rates (**Fig. 2d**). While wind speed was generally low, wind direction changed throughout the day, which may have led to temporal and spatial differences in wind-driven gas transfer and water transport that modified the effect of vegetation. In contrast to lateral variability, no vertical gradients in water column properties were detected.

3.3 Daily to seasonal environmental variability

Oxygen production covaried with PAR, temperature, tidal stage, and winds over the seasonal time series. In particular, GOP and R tracked both short and long term variations in PAR and were suppressed by biweekly periods of spring-tide flooding (Figure S2 in **Online Resource S2**)

and potential connectivity to the broader marsh (Spivak et al. 2017). The response of GOP, NEM, and R to daily to weekly scale environmental variability was evaluated using an ARIMA procedure (Table S3 in **Online Resources S3**; the following summary notes significant correlations, $p<0.05$). GOP_{O2} and R were significantly, positively correlated with PAR, and negatively correlated with windspeed and recent tidal flooding. GOP_{O2} was also significantly correlated with wind direction; onshore, westerly winds were associated with greater GOP_{O2}. Onshore winds tend to correspond to fewer clouds and thus higher PAR ($r=0.31$ for correlation between wind direction and PAR, $p=4\times10^{-5}$). Neither R nor GOP_{O2} was correlated with daily to weekly variability in temperature. Correlations with PAR, winds, and flooding only accounted for 27% of the variance in R and 51% of the variance in GOP_{O2}.

In contrast to GOP_{O2}, GOP_{TOI} was not generally correlated with daily to weekly variability in PAR, despite tracking PAR closely at hourly scales, nor was it correlated with the other environmental variables. GOP_{O2} was calculated from R and thus these rates were highly cross-correlated ($r=0.79$, $p=3\times10^{-26}$), but independently measured GOP_{TOI} was also significantly correlated with R ($r=0.63$, $p=6\times10^{-3}$). These cross-correlations between GOP and R accounted for a greater share of the total variance than accounted for by the measured environmental variables. Thus as yet untested factors may underpin the daily to weekly variability in rates from each method—ebullition is one likely driver of differences between the two methods over daily time scales (Howard et al. 2018). However, an important caveat is that daily GOP_{TOI} rates were evaluated over only 10% of the overall time series (17 of 174 days), limiting our statistical power.

4. Discussion

443 *4.1 Convergent rates of daily to seasonal GOP*

444 Mean daily rates of GOP_{TOI} and GOP_{O2} broadly agreed over the time series, with similar
445 seasonal trends (**Fig. 2d**) and no significant bias (**Fig. 3c**). The mean ratio of
446 GOP_{TOI}/GOP_{O2}=1.0(0.4). This is similar to the mean and range of ratios calculated in pelagic
447 ocean Lagrangian experiments (Hamme et al. 2012) and estuarine benthic chambers (Stanley and
448 Howard 2013). This agreement implies that even in a setting expected to favor light-dependent
449 O_2 uptake, the contributions of such processes at daily to seasonal time scales are not large
450 compared to the relative methodological uncertainties (on average, 10% of GOP).

451 There were exceptions to this broad agreement. Eight of the daily GOP_{TOI} rates (**Fig. 2d**) differed
452 from GOP_{O2} by a larger degree than could be explained by methodological uncertainties (>2
453 standard deviations). However, these differences were not consistent with a major role for light-
454 dependent O_2 uptake; larger GOP differences were not systematically distributed over the time
455 series with respect to seasonal trends or daily changes in PAR. Instead, environmental
456 heterogeneity associated with vegetation likely contributed to periods with larger than expected
457 rate differences between GOP_{TOI} at the sample locations and GOP_{O2} at the sensor location.

458 Temperature and O_2 varied by tens of percent around the pond margins, suggesting that this
459 setting was not always well-mixed despite the lack of vertical gradients. Submerged aquatic
460 vegetation reduces turbulence and increases mixing time scales (Koch and Gust 1999, Romano et
461 al. 2003, Nepf and Ghisalberti 2008). In addition, *U. intestinalis* mats likely limited air-water gas
462 exchange (e.g. Wollenberg and Peters 2009, Attermeyer et al. 2016) and enhanced accumulation
463 of photosynthetic oxygen compared to unvegetated areas. Vegetation likely also contributed to
464 variability in important O_2 sinks in this pond such as ebullition from photosynthetic surfaces
465 (Howard et al. 2018) and the sedimentary uptake dominating the net metabolism of the pond

(e.g., sulfide oxidation; Spivak et al. 2018). Thus we infer that the heterogeneity in vegetation cover, and resulting biological and physical impacts on O_2 dynamics, contributed to variability in production rates around the pond. In larger lakes, spatial heterogeneity in temperature and oxygen can lead to highly variable estimates of gross productivity and respiration (Van de Bogert 2012), and submerged aquatic vegetation strongly influences these environmental drivers (Vilas et al. 2017). This is also consistent with the important role of vegetation cover in explaining variability in metabolism rates between salt marsh ponds (Spivak et al. 2017).

4.2 Light-dependent effects on rates of hourly GOP

In contrast to the daily rates, there were systematic discrepancies in hourly rates of GOP_{TOI} and GOP_{O2} during midday periods which could reflect light-dependent processes. There was a small but significant bias between GOP_{TOI} and GOP_{O2} (**Figs. 2a-c**, **3a**). This resulted in a ratio of hourly GOP_{TOI}/GOP_{O2} equal to 1.4(1.7). The variability in this ratio was increased compared to daily rates in part because of the large relative uncertainty associated with near-zero dawn and dusk GOP rates; the ratio derived from only the highest production rate on each day was 1.5(0.6). This poorer agreement during periods of peak production was not a function of lags between the GOP rates—instead, the GOP_{TOI}-GOP_{O2} difference was correlated with hourly fluctuations in the magnitude of production and PAR (section *3.1*). These relationships point to a potential small but observable divergence of hourly GOP rates due to light-dependent O_2 uptake. The greater GOP_{TOI} relative to GOP_{O2} was consistent with the expected effects of plausible light-dependent processes (**Table 1**), and within the range of the 23-62% difference expected if light-dependent O_2 uptake were 2-10 times greater than in the dark (e.g., Bender et al. 1987, Epping and Jørgensen 1996, Pringault et al. 2009). This ratio was greater than could be explained by the expected uncertainties in the difference between hourly rates (on average, 16% of GOP).

Daytime oxidation of reduced compounds produced overnight in the sediments (Fenchel and Glud 2000) is likely in shallow pond sediments, but would be expected to cause GOP rates to diverge most in the morning. Photorespiration would cause GOP rates to diverge most in the afternoon when the ratio of O_2 to carbon dioxide is highest in this pond (Howard 2017) and nearby shallower pools (Koop-Jakobsen and Gutbrod 2019). Instead, the GOP_{TOI}-GOP_{O2} difference is greatest at peak production and PAR. Light-stimulation of mitochondrial respiration can cause GOP_{O2} to underestimate productivity, and contributes to both autotrophic and heterotrophic carbon metabolism at ecosystem scales (Grande et al. 1989, Pringault et al. 2009). In contrast, photoreduction, or the Mehler reaction, is largely decoupled from carbon metabolism (Williams and del Giorgio 2005), and may primarily serve to remove excess electrons at the cellular level (Raven and Beardall 2005). Photoreduction reduces O_2 to water at photosystem I (PSI), and can be a major oxygen uptake flux for autotrophs in the light, consuming the equivalent of 10-75% of photosystem II (PSII) O_2 output (Milligan et al. 2007, Halsey et al. 2010, Roberty et al. 2014) and causing GOP_{TOI} to overestimate productivity. Both processes could lead to the observed midday divergence between GOP_{TOI} and GOP_{O2} (**Online Resource S2**).

However, as with the daily GOP rates, environmental heterogeneity at hourly scales may play a large role in this setting, and the limited spatial resolution across the pond makes it difficult to confirm that the observed differences at short time scales are mainly due to light-dependent processes. Ebullition in particular, where active, may lead to divergent GOP_{O2} and GOP_{TOI} in the midday and afternoon when most bubbles escape (Howard et al. 2018).

4.3 Daytime production and net ecosystem metabolism

511 The pond in this study was shallow and heterotrophic on daily to seasonal time scales, but
512 autotrophic during the daytime. This metabolic dynamism may contribute to our seemingly
513 contradictory findings of a potential role of light-dependent O_2 uptake over short periods during
514 autotrophic daytime periods, but no effect over daily to seasonal periods; large, light-insensitive
515 respiration rates could mask smaller light-dependent fluxes when integrated over longer time
516 periods. Midday (~ 3 h) chamber experiments found lower rates of respiration and a more
517 autotrophic balance of production and respiration in surface waters than in chambers overlying
518 sediments (Howard 2017). GOP_{TOI} and GOP_{O2} agreed in chambers over microalgal and
519 macroalgal covered sediments, and the metabolism of suspended microalgae was minor
520 compared to sedimentary fluxes. Thus, potential light-dependent differences may arise from
521 portions of the pond with *R. maritima*.

522 Prior work in this and other salt marsh ponds showed that organic-rich sediments support high
523 rates of ecosystem respiration (Spivak et al. 2017), through both aerobic and anaerobic pathways
524 including microbial sulfur cycling (Wilbanks et al. 2014, Rao et al. 2016, Spivak et al. 2018).
525 Thus reduced compounds in pond sediments have the potential to consume much of the O_2
526 produced during daytime periods of water column autotrophy. This point is illustrated by
527 comparing ratios of NEM/GOP (**Fig. 6**); during daylight periods ratios were ~ 0 (using GOP
528 from either method), indicating that as much O_2 was consumed as was produced. Over 24 hours,
529 nighttime O_2 uptake pushed the system to net heterotrophy (NEM/GOP ~ -0.4, i.e. respiration
530 exceeded production by 40%). The net result that NEM varied little over the six-month study
531 period (**Fig. 2d**) is underlain by a steady background of sedimentary O_2 uptake. Concurrent
532 assessments of microbial activity in this pond also point to more stable sediment conditions
533 compared to the overlying water column; microbial activity in the water column was strongly

associated with diel changes in environmental conditions, but microbial communities in surficial sediments were insensitive to changes in overlying temperature and O_2 (Kearns et al. 2017).

5. Conclusions

The TOI method was expected to highlight light-dependent processes that could affect GOP estimates from dissolved O_2 mass balances. On daily to seasonal time scales, we found good overall agreement between daily to seasonal rates GOP_{TOI} and GOP_{O2}, despite a number of environmental factors expected to cause light-dependent O_2 uptake. This agreement may reflect the strong heterotrophy and dominance of sedimentary respiration in this shallow pond, which consumed more O_2 than photosynthetically produced.

Hourly GOP rates within individual days did exhibit discrepancies between the methods that were consistent with light-dependent processes. Given the ambiguous importance of light-dependent O_2 uptake in this setting, we could not disentangle the potential light-dependent processes affecting our results. However, photoreduction or light-stimulated mitochondrial respiration are likely processes in this setting that are consistent with the observed O_2 dynamics.

Ultimately, the importance of daily to seasonal agreement (or hourly disagreement) between the TOI and dissolved O_2 mass balance methods depends upon the research question. The hourly time series in this study point to isotopic method having sufficient resolution to study light-dependent O_2 uptake processes in a common O_2 currency with a dissolved mass balance. In a setting with smaller respiratory fluxes these differences would be proportionally larger, which could contribute to the high ratios of light versus dark respiration reported for other environments (e.g., Bender et al. 1987). However, the typical use of dissolved O_2 mass balances

556 is to study ecosystem metabolism fluxes over daily to yearly time scales. In this salt marsh pond,
557 the daily production rates derived from the TOI method agreed with those from the dissolved O_2
558 mass balance. Our results support the typical assumption that daytime and nighttime rates of O_2
559 consumption rates are similar, at least in environments where light-independent sediment
560 respiration dominates ecosystem metabolism. Thus we view the TOI method, with additional
561 analytical requirements, as being best suited for targeted process studies rather than routine
562 monitoring in aquatic environments in which dissolved O_2 sensors can be readily deployed and
563 maintained. For pelagic locations where instrumentation is not practical (e.g. infrequently
564 occupied hydrographic stations), this work suggests that the TOI method can provide a good
565 alternative for evaluating *in situ* oxygen production.

566 The heterogeneity of production over small spatial scales around this small pond is an important
567 additional finding. This contributes to the growing understanding that even very shallow aquatic
568 environments may not be well-mixed (e.g., Holgerson et al. 2016), which can complicate
569 interpretation of biogeochemical tracers and drive substantial spatial heterogeneity in metabolic
570 rates (Van de Bogert et al. 2012).

571

572 Acknowledgements

573 This work depended on the outstanding logistical and in-kind support of the Plum Island
574 Ecosystems Long Term Ecological Research site and TIDE experiment staff and scientists
575 (National Science Foundation (NSF) OCE 1238212, NSF DEB 1354494, and Northeast Climate
576 Science Center grant DOI G12-AC00001). We thank Nancy Pau and the Parker River National
577 Wildlife Refuge for permitting, and Jeanine Ash and one anonymous reviewer for thoughtful

feedback on the manuscript. E.M.H. was supported by the National Defense Science and Engineering Graduate Fellowship. Funding for this research and support for A.C.S. and R.H.R.S. was provided by NSF OCE 1233678. Additional support to A.C.S was provided by Woods Hole Sea Grant (NA14OAR4170104) and the National Oceanic and Atmospheric Administration and National Estuarine Research Reserve System Science Collaborative (NA14NOS4190145). J.S.K. was supported by the Woods Hole Oceanographic Institution (WHOI) Summer Student Fellowship program. E.M.H., A.C.S., and R.H.R.S. developed the isotopic time series study. E.M.H. and A.C.S. wrote the manuscript. All authors contributed to sample collection, sample analysis, and/or data interpretation, and commented on manuscript drafts. The authors have no real or perceived financial or affiliation-related conflicts of interest with respect to the results of this paper. Ancillary meteorological data are accessible from the LTER Network Information System Data Portal (https://doi-org /10.6073/pasta/14eb405f583ae2384b2c6c5714776214). The dissolved oxygen and other environmental time series collected from sensor deployments are accessible from the Biological and Chemical Oceanography Data Management Office (https://www.bco-dmo.org/dataset/670819). Other data used in this work (e.g. isotopic ratios) are provided in the supplementary materials available with the electronic version of this paper.

References

Abe, O., and N. Yoshida. 2003. Partial pressure dependency of $^{17}O/^{16}O$ and $^{18}O/^{16}O$ of molecular oxygen in the mass spectrometer. *Rapid Comm. Mass Spectrom*. 17(5): 395–400. doi: 10.1002/rcm.923

Angert, A., S. Rachmilevitch, E. Barkan, and B. Luz. 2003. Effects of photorespiration, the cytochrome pathway, and the alternative pathway on the triple isotopic composition of atmospheric O_2. *Glob. Biogeochem. Cycles* 17(1): 1030. doi: 0.1029/2002GB00193

601 Attermeyer, K., S. Flury, R. Jayakumar, P. Fiener, K. Steger, V. Arya, F. Wilken, R. van
602 Geldern, and K. Premke. 2016. Invasive floating macrophytes reduce greenhouse gas emissions
603 from a small tropical lake. *Sci. Rep.* 6: 20424. doi: 10.1038/srep20424

604 Bender, M., K. Grande, K. Johnson, J. Marra, P.J.L.B. Williams, J. Sieburth, M. Pilson, C.
605 Langdon, G. Hitchcock, J. Orchardo, C. Hunt, P. Donaghay, and K. Heinemann. 1987. A
606 comparison of four different methods for determining planktonic community production. *Limnol.*
607 *Oceanogr.* 32(5): 1085-1098. doi: 10.4319/lo.1987.32.5.1085

608 Benson, B.B., and D. Krause Jr. 1980. The concentration and isotopic fractionation of gases
609 dissolved in freshwater in equilibrium with the atmosphere: 1. Oxygen. *Limnol. Oceanogr.*
610 25(4): 662-671. doi: 10.4319/lo.1980.25.4.0662

611 Benson, B.B., and D. Krause Jr. 1984. The concentration and isotopic fractionation of oxygen
612 dissolved in freshwater and seawater in equilibrium with the atmosphere. *Limnol. Oceanogr.*
613 29(3): 620-632. doi: 10.4319/lo.1984.29.3.0620

614 Buapet, P., L.M. Rasmusson, M. Gullström, and M. Björk. 2013. Photorespiration and carbon
615 limitation determine productivity in temperate seagrasses.

616 Caffrey, J.M. 2004. Factors controlling net ecosystem metabolism in U.S. estuaries. *Estuar.*
617 *Coasts* 27(1): 90-101. doi: 10.1007/BF02803563

618 Demars, B.O.L., J. Thompson, and J.R. Manson. 2015. Stream metabolism and the open diel
619 oxygen method: Principles, practice, and perspectives. *Limnol. Oceanogr. Methods* 13(7): 356-
620 374. doi: 10.1002/lom3.10030

621 D'Errico, J. 2012. inpaint_nans v.1.1. Matlab File Exchange.
622 https://www.mathworks.com/matlabcentral/fileexchange/4551-inpaint_nans. Accessed 1 August
623 2017.

624 Eisenstadt, D., E. Barkan, B. Luz, and A. Kaplan. 2010. Enrichment of oxygen heavy isotopes
625 during photosynthesis in phytoplankton. *Photosynth. Res.* 103: 97-103. doi: 10.1007/s11120-
626 009-9518-z

627 Epping, E.H.G., and B.B. Jørgensen. 1996. Light-enhanced oxygen respiration in benthic
628 phototrophic communities. *Mar. Ecol. Prog. Ser.* 139: 193-203. doi: 10.3354/meps139193

629 Falkowski, P.G., and T.G. Owens. 1978. Effects of light intensity on photosynthesis and dark
630 respiration in six species of marine phytoplankton. *Mar. Biol.* 45(4): 289-295. doi:
631 10.1007/BF00391815

632 Falkowski, P.G., and J.A. Raven. 1997. *Aquatic photosynthesis*. Paris: Blackwell Science.

633 Fenchel, T., and R.N. Glud. 2000. Benthic primary production and O_2-CO_2 dynamics in a
634 shallow-water sediment: Spatial and temporal heterogeneity. *Ophelia* 53(2): 159-171. doi:
635 10.1080/00785236.2000.10409446

636 Forbrich, I., and A.E. Giblin. 2015. Marsh-atmosphere CO_2 exchange in a New England salt
637 marsh. *J. Geophys, Res. Biogeosci.* 120(9): 1825-1838. doi: 10.1002/2015JG003044

638 Garcia, H.E., and L.I. Gordon. 1992. Oxygen solubility in seawater: Better fitting equations.
639 *Limnol. Oceanogr.* 37(6): 1307-1312. doi: 10.4319/lo.1992.37.6.1307

640 Garcia, H.E., and L.I. Gordon. 1993. Erratum: Oxygen solubility in seawater: Better fitting
641 equations. *Limnol. Oceanogr.* 38(3): 656. doi: 10.4319/lo.1993.38.3.0643

642 Grande, K.D., J. Marra, C. Langdon, K. Heinemann, and M.L. Bender. 1989. Rates of respiration
643 in the light measured in marine phytoplankton using an ^{18}O isotope-labeling technique. *J. Exper.*
644 *Mar. Biol. Ecol.* 129(2): 95-120. doi: 10.1016/0022-0981(89)90050-6

645 Halsey, K.H., A.J. Milligan, and M.J. Behrenfeld. 2010. Physiological optimization underlies
646 growth rate-independent chlorophyll-specific gross and net primary production. *Photosynth. Res.*
647 103(2): 125-137. doi: 10.1007/s11120-009-9526-z

648 Hamme, R.C., N. Cassar, V.P. Lance, R.D. Vaillancourt, M.L. Bender, P.G. Strutton, T.S.
649 Moore, M.D. DeGrandpre, C.L. Sabine, D.T. Ho, and B.R. Hargreaves. 2012. Dissolved O_2/Ar
650 and other methods reveal rapid changes in productivity during a Lagrangian experiment in the
651 Southern Ocean. *J. Geophys. Res. Oceans* 117(C00F12): 1-19. doi: 10.1029/2011JC007046.

652 Helman, Y., E. Barkan, D. Eisenstadt, and A. Kaplan. 2005. Fractionation of the three stable
653 oxygen isotopes by oxygen-producing and oxygen-consuming reactions in photosynthetic
654 organisms. *Plant Physiol.* 138(4): 2292-2298. doi: 10.1104/pp.105.063768

655 Holgerson, M.A., C.J. Zappa, and P.A. Raymond. 2016. Substantial overnight reaeration by
656 convective cooling discovered in pond ecosystems. *Geophys. Res. Lett.* 43(15): 8044-8051. doi:
657 10.1002/2016GL070206

658 Holtgrieve, G.W., D.E. Schindler, T.A. Branch, and Z.T. A'mar. 2010. Simultaneous
659 quantification of aquatic metabolism and reaeration using a Bayesian statistical model of oxygen
660 dynamics. *Limnol. Oceanogr.* 55(3): 1047-1063. doi: 10.4319/lo.2010.55.3.1047

661 Howard, E.M. 2017. *Ecosystem metabolism in salt marsh tidal creeks and ponds: Applying triple*
662 *oxygen isotopes and other gas tracers to novel environments*. 69-70, 135-172. Woods Hole, MA:

663 PhD thesis submitted to the Massachusetts Institute of Technology and the Woods Hole
664 Oceanographic Institution. doi: 10.1575/1912/8654

665 Howard, E.M., I. Forbrich, A.E. Giblin, D.E. Lott III, K.L. Cahill, and R.H.R. Stanley. 2018.
666 Using noble gases to compare parameterizations of air-water gas exchange and to constrain
667 oxygen losses by ebullition in a shallow aquatic environment. *J. Geophys. Res. Biogeosci.*
668 123(9): 2711-2726. doi: 10.1029/2018JG004441

669 Juranek, L.W., and P.D. Quay. 2013. Using triple isotopes of dissolved oxygen to evaluate global
670 marine productivity. *Annu. Rev. Mar. Sci.* 5: 503-524. doi: 10.1146/annurev-marine-121211-
671 172430

672 Kaiser, J. 2011. Technical note: Consistent calculation of aquatic gross production from oxygen
673 triple isotope measurements. *Biogeosci.* 8(7): 1793-1811. doi: 10.5194/bg-8-1793-2011

674 Kaiser, J., and O. Abe. 2012. Reply to Nicholson's comment on "Consistent calculation of
675 aquatic gross production from oxygen triple isotope measurements" by Kaiser (2011). *Biogeosci.*
676 9(8): 2993-2997. doi: doi.org/10.5194/bg-8-2993-2011

677 Kana, T.M. 1990. Light-dependent oxygen cycling measured by an oxygen-18 isotope dilution
678 technique. *Mar. Ecol. Prog. Ser.* 64: 293-300. doi: 10.3354/meps064293

679 Kearns, P.J., D. Holloway, H.H. Angell, S.G. Feinman, J.L. Bowen. 2017. Effect of short-term,
680 diel changes in environmental conditions on active microbial communities in a salt marsh pond.
681 *Aquat. Microb. Ecol.* 80(1): 29-41. doi: 10.3354/ame01837

682 Keeling, R.F., A.C. Manning, E.M. McEvoy, and S.R. Shertz. 1998. Methods for measuring
683 changes in atmospheric O_2 concentration and their application in southern hemisphere air. *J.*
684 *Geophys. Res.* 103(D3): 3381-3397. doi: 10.1029/97JD02537

685 Koch, E.W., and G. Gust. 1999. Water flow in tide- and wave-dominated beds of the seagrass
686 *Thalassia testudinum*. *Mar. Ecol. Prog. Ser.* 184: 63-72. doi: 10.3354/meps184063

687 Koop-Jakobsen, K., and M.S. Gutbrod. 2019. Shallow salt marsh tidal ponds—an environment
688 with extreme oxygen dynamics. *Front. Environ. Sci.* 7(137): 1-14. doi:
689 10.3389/fenvs.2019.00137

690 Laws, E.A., M.R. Landry, R.T. Barber, L. Campbell, M-L. Dickson, and J. Marra. 2000. Carbon
691 cycling in primary production bottle incubations: inferences from grazing experiments and
692 photosynthetic studies using ^{14}C and ^{18}O in the Arabian Sea. *Deep Sea Res. II* 47(7): 1339-1352.
693 doi: 10.1016/S0967-0645(99)00146-0

694 Li, B., L.Y. Yeung, H. Hu, and J.L. Ash. 2019. Kinetic and equilibrium fractionation of O_2
695 isotopologues during air-water gas transfer and implications for tracing oxygen cycling in the
696 ocean. *Mar. Chem.* 210: 61-71. doi: 10.1016/j.marchem.2019.02.006

697 Luz, B., and E. Barkan. 2000. Assessment of oceanic productivity with the triple-isotope
698 composition of dissolved oxygen. *Science* 288(5473): 2028-2031. doi:
699 10.1126/science.288.5473.2028

700 Luz, B., and E. Barkan. 2005. The isotopic ratios $^{17}O/^{16}O$ and $^{18}O/^{16}O$ in molecular oxygen and
701 their significance in biogeochemistry. *Geochimica et Cosmochimica Acta* 69(5): 1099-1110. doi:
702 10.1016/j.gca.2004.09.001

703 Luz, B., and E. Barkan. 2011. Proper estimation of marine gross O_2 production with $^{17}O/^{16}O$ and
704 $^{18}O/^{16}O$ ratios of dissolved O_2. *Geophys. Res. Lett.* 38(19): L19606. doi:10.1029/2011GL049138

705 Manning, C.C., and E.M. Howard. 2017. calcGOP: Functions for calculating gross oxygen
706 production from measurements of the triple oxygen isotopic composition of dissolved O_2.
707 http://github.com/caramanning/calcGOP, release 1.0.

708 Manning, C.C., E.M. Howard, D.P. Nicholson, B.Y. Ji, Z.O. Sandwith, and R.H.R. Stanley.
709 2017. Revising estimates of aquatic gross oxygen production by the triple oxygen isotope
710 method to incorporate the local isotopic composition of water. *Geophys. Res. Lett.* 44(20):
711 10511-10519. doi: 10.1002/2017GL074375

712 Milligan, A.J., I. Berman-Frank, Y. Gerchman, G.C. Dismukes, and P.G. Falkowski. 2007.
713 Light-dependent oxygen consumption in nitrogen-fixing cyanobacteria plays a key role in
714 nitrogenase protection. *J. Phycol.* 43(5): 845-852. doi: 10.1111/j.1529-8817.2007.00395.x

715 Nepf, H., and M. Ghisalberti. 2008. Flow and transport in channels with submerged vegetation.
716 *Acta Geophsica* 56(3): 753-777. doi: 10.2478/s11600-008-0017-y

717 Nicholson, D.P. 2011. Comment on: "Technical note: Consistent calculation of aquatic gross
718 production from oxygen triple isotope measurements" by Kaiser (2011). *Biogeosci.* 8(10): 2993-
719 2997. doi: 10.5194/bg-8-2993-2011

720 Odum, H.T. 1956. Primary production in flowing waters. *Limnol. Oceanogr.* 1(2): 102-117. doi:
721 10.4319/lo.1956.1.2.0102

722 Parkhill, K.L., and J.S. Gulliver. 1998. Application of photorespiration concepts to whole stream
723 productivity. *Hydrobiologia* 389(1): 7-19. doi: 10.1023/A:1003519302002

724 Pringault, O., S. Tesson, and E. Rochelle-Newall. 2009. Respiration in the light and bacterio-
725 phytoplankton coupling in a coastal environment. *Microb. Ecol.* 57(2): 321-334. doi:
726 10.1007/s00248-008-9422-7

727 Prokopenko, M.G., O.M. Pauluis, J. Granger, and L.Y. Yeung. 2011. Exact evaluation of gross
728 photosynthetic production from the oxygen triple-isotope composition of O_2: Implications for the
729 net-to-gross primary production ratios. *Geophys, Res. Lett.* 38(14): L14603. doi:
730 10.1029/2011GL047652

731 Rao, A., N. Risgaard-Petersen, and U. Neumeier. 2016. Electrogenic sulfur oxidation in a
732 northern saltmarsh (St. Lawrence Estuary, Canada). *Canad. J. Microbiol.* 62(6): 530-537. doi:
733 10.1139/cjm-2015-0748

734 Raven, J.A., and J. Beardall. 2005. Respiration in aquatic photolithotrophs. In *Respiration in*
735 *Aquatic Ecosystems*, eds. del Giorgio and Williams, 36-46. Oxford: Ocford U. Press.

736 Reuer, M.K., B.A. Barnett, M.L. Bender, P.G. Falkowski, and M.B. Hendricks. 2007. New
737 estimates of Southern Ocean biological production rates from O_2/Ar ratios and the triple isotope
738 composition of O_2. *Deep Sea Res. I* 54(6): 951-974. doi: 10.1016/j.dsr.2007.02.007

739 Roberty, S., B. Bailleul, N. Berne, F. Franck, and P. Cardol. 2014. PSI Mehler reaction is the
740 main alternative photosynthetic electron pathway in Symbiodinium sp., symbiotic dinoflagellates
741 of cnidarians. *New Phytologist* 204(1): 81-91. doi: 10.1111/nph.12903

742 Romano, C., J. Widdows, M.D. Brinsley, and F.J. Staff. 2003. Impact of *Enteromorpha*
743 *intestinalis* mats on near-bed currents and sediment dynamics: Flume studies. *Mar. Ecol. Prog.*
744 *Ser.* 256: 63-74. doi: 10.3354/meps256063

Sarma, V.V.S.S., O. Abe, S. Hashimoto, A. Hinuma. and T. Saino. 2005. Seasonal variations in triple oxygen isotopes and gross oxygen production in the Sagami Bay, central Japan. *Limnol. Oceanogr.* 50(2): 544-552. doi: 10.4319/lo.2005.50.2.0544

Spivak, A.C., K. Gosselin, E.M. Howard, G. Mariotti, I. Forcrich, R.H.R. Stanley, and S.P. Sylva. 2017. Shallow ponds are heterogeneous habitat within a temperate salt marsh ecosystem. *J. Geophys. Res. Biogeoscie.* 122(6): 1371-1384. doi: 10.1002/2017JG003780

Spivak, A.C., K. Gosselin, and S.P. Sylva. 2018. Shallow ponds are biogeochemically distinct habitats in salt marsh ecosystems. *Limnol. Oceanogr.* 63(4): 1622-1643. doi: 10.1002/lno.10797

Staehr, P.A., D. Bade, M.C. Van de Bogert, G.R. Koch, C. Williamson, P. Hanson, J.J. Cole, and T. Kratz. 2010. Lake metabolism and the diel oxygen technique: State of the science. *Limnol. Oceanogr. Methods* 8(11): 628-644. doi: 10.4319/lom.2010.8.0628

Stanley, R.H.R., and E.M. Howard. 2013. Quantifying photosynthetic rates of microphytobenthos using the triple isotope composition of dissolved oxygen. *Limnol. Oceanogr. Methods* 11: 360-373. doi: 10.4319/lom.2013.11.360

Stanley, R. H. R., J. B. Kirkpatrick, N. Cassar, B. A. Barnett, and M. L. Bender. 2010. Net community production and gross primary production rates in the western equatorial Pacific. *Glob. Biogeochem. Cycles* 24(4): GB4001. doi:10.1029/2009GB003651

Suggett, D.J., H.L. MacIntyre, T.M. Kana, and R.J. Geider. 2009. Comparing electron transport with gas exchange: Parameterising exchange rates between alternative photosynthetic currencies for eukaryotic phytoplankton. *Aquat. Microb. Ecol.* 56: 147-162. doi: 10.3354/ame01303

765 Wilbanks, E.G., U. Jaekel, V. Salman, P.T. Humphrey, J.A. Eisen, M.T. Facciotti, D.H.
766 Buckley, S.H. Zinder, G.K. Druschel, D.A. Fike, and V.J. Orphan. 2014. Microscale sulfur
767 cycling in the phototrophic pink berry consortia of the Sippewissett Salt Marsh. *Environ.*
768 *Microbiol.* 16(11): 3398-3415. doi: 10.1111/1462-2920.12388

769 Winslow, L.A., J.A. Zwart, R.D. Batt, H.A. Dugan, R.I. Woolway, J.R. Corman, P.C. Hanson,
770 and J.S. Read. 2016. LakeMetabolizer: an R package for estimating lake metabolism from free-
771 water oxygen using diverse statistical models. *Inland Waters* 6(4): 622-636. doi: 10.5268/IW-
772 6.4.883

773 Thiemens, M.H. 2001. The mass-independent ozone isotope effect. *Science* 293(5528): 226. doi:
774 10.1126/science.1063648

775 Vachon, D., and Y.T. Prairie. 2013. The ecosystem size and shape dependence of gas transfer
776 velocity versus wind speed relationships in lakes. *Canadian J. Fish. Aquat. Sci.* 70(12): 1757-
777 1764. doi: 10.1139/cjfas-2013-0241

778 Van de Bogert, M.C., D.L. Bade, S.R. Carpenter, J.J. Cole, M.L. Pace, P.C. Hanson, and O.C.
779 Langman. 2012. Spatial heterogeneity strongly affects estimates of ecosystem metabolism in two
780 north temperate lakes. *Limnol. Oceanogr.* 57(6): 1689-1700. doi: 10.4319/lo.2012.57.6.1689

781 Vilas, M.P., C.L. Marti, M.P. Adams, C.E. Oldham, and M.R. Hipsey. 2017. Invasive
782 macrophytes control the spatial and temporal patterns of temperature and dissolved oxygen in a
783 shallow lake: A proposed feedback mechanism of macrophytes loss. *Front. Plant Sci.* 8:2097.
784 doi: 10.3389/fpls.2017.02097

785 Williams, P.J. le B., and P.A. del Giorgio. Respiration in aquatic ecosystems: history and
786 background. In *Respiration in aquatic ecosystems*, eds. del Giorgio and Williams, 1-17. Oxford:
787 Oxford U. Press.

788 Wollenberg, J.L., and S.C. Peters. 2009. Diminished mercury emission from waters with
789 duckweed cover. *J. Geophys. Res. Biogeosci.* 114(G2): G00C08. doi: 10.1029/2008JG000770

790 Yang, B., S.R. Emerson, and S.M. Bushinsky. 2017. Annual net community production in the
791 subtropical Pacific Ocean from *in situ* oxygen measurements on profiling floats. *Glob.*
792 *Biogeochem. Cycles* 31(4): 728-744. doi: 10.1002/2016GB005545

793 Yvon-Durocher, G., J.M. Caffrey, A. Cescatti, M. Dossena, P. del Giorgio, J.N. Gasol, J.M.
794 Montoya, J. Pumpanen, P.A. Staehr, M. Trimmer, G. Woodward, and A.P. Allen. 2012.
795 Reconciling the temperature dependence of respiration across timescales and ecosystem types.
796 *Nature* 487: 472-476. doi: 10.1038/nature11205

797

Table 1. Sources of light-dependent divergence in gross oxygen production

Light-dependent oxygen update processes that could lead to divergence in gross oxygen production derived from the diel dissolved oxygen mass balance and the triple oxygen isotope method (GOP_{O2} and GOP_{TOI}). Also, the time of day the two GOP rates are expected to diverge most if a particular process leads to observable differences. These processes are discussed in greater detail in **Online Resource S2**.

Process	Effect on GOP: GOP_{O2}	GOP_{TOI}	Greatest daytime difference:
Photoreduction	No change	Overestimate	Midday, at high light
Photorespiration	Underestimate	No change	In afternoon, when partial pressures of O_2 are highest and CO_2 lowest
Light-stimulated autotrophic respiration	Underestimate	No change	Midday, at high productivity
Indirect stimulation of heterotrophic respiration	Underestimate	No change	Midday, at high productivity
Oxidation of sediment compounds	Underestimate	No change or underestimate[a]	In morning, after overnight accumulation of sediment oxygen debt

[a] Dissolved oxygen that is completely produced and consumed within the sediments will not influence the isotopic characteristics of the bulk O_2 pool measured in the water column, which could cause both GOP rates to underestimate daytime productivity and diverge by less. See **Online Resource S2**).

Figure captions

Figure 1. Sample locations and vegetation cover

Map of sensor (S, red square) and sample locations (numbers, red circles). North is top of figure. Light red circles indicate locations where a subset of tracers were sampled, but GOP_{TOI} was not evaluated. Gray shading and colorbar indicates vegetation cover, averaged over the seasonal sampling period, and interpolated or extrapolated over a 5 x 5 m^2 resolution grid (see text). Sensor was located over unvegetated sediment, but was within 2-3 m of vegetation cover. The southernmost portion of the pond near sample location 4 had some vegetation, but was not quantitatively surveyed.

Figure 2. Hourly and daily ecosystem metabolism rates

Rates of gross oxygen production, GOP_{O2} (red line and shaded one standard deviation error bounds) and GOP_{TOI} (red circles and black one standard deviation error bars), dark respiration and sediment oxygen uptake, R (black line and shaded error bounds), and net ecosystem metabolism, NEM (blue line and shaded error bounds). Shaded error bars do not include systematic errors shared by the dissolved oxygen mass balance and triple oxygen isotope methods. (**a-c**) Hourly-scale rates plotted against photosynthetically active radiation (PAR, orange line) on three days with at least four GOP_{TOI} rates. Here R is inferred to equal average NEM during nighttime periods (grey shaded periods). (**d**) Daily mean rates (same units as **a-c**). Numbers above GOP_{TOI} daily rates indicate the sample location from **Fig. 1**. GOP_{TOI} daily rates are scaled from at least two midday, hourly-scale rates using PAR (see text).

Figure 3. Gross oxygen production rate comparisons

Differences in (**a**, **b**) hourly and (**c**, **d**) daily rates of gross oxygen production from the triple oxygen isotope and dissolved oxygen mass balance methods (GOP_{TOI} and GOP_{O2}), plotted against the average GOP rate from both methods over concurrent periods. Individual daily or hourly rate differences are plotted as either absolute (GOP_{TOI}-GOP_{O2}, mmol O_2 m^{-2} h^{-1} for either period) or relative differences ([GOP_{TOI}-GOP_{O2}]/mean[GOP_{TOI}, GOP_{O2}]). One standard deviation error bars are in blue. Mean GOP_{TOI} - GOP_{O2} rate difference (bias) is marked with a solid black line (*p* value noted for null hypothesis of no bias), and 95% confidence intervals (limits of agreement) with dashed black lines. Both the absolute and relative hourly rate differences are significantly correlated to the magnitude of production (grey lines and text, with reported *p* reported for linear regression with null hypothesis of no correlation), while the daily rates are not (see text in panels for *r* and *p*). In panel **b** (**inset**), the near zero rate leads to large divergence (-27 relative difference) and relative errors (standard deviation of 193) despite the good constraints on the absolute rate. Because this reflects numerical rather than methodological uncertainty, this point is not included in the calculation of bias, limits of agreement, or the regression of relative rate differences against mean GOP. Including this relative rate does not alter the conclusions.

Figure 4. Spatial variability of temperature, oxygen, and triple oxygen isotope ratios

Morning (left column) and afternoon (right column) values of environmental variables around the pond (filled, colored circles) on May 29 2014, superimposed on vegetation cover map (grayscale). Mean wind direction and speed (standard deviation in parentheses) for each period is followed by (**a-b**) temperature, (**c-d**) dissolved oxygen saturation relative to atmospheric

equilibrium, (**e-f**) the triple oxygen isotope tracer of oxygen derived from photosynthesis relative to air-water gas exchange, $^{17}\Delta$.

Figure 5. Seasonal variability in dissolved oxygen rate of increase

Effect size of variability in rate of morning to afternoon increase in dissolved oxygen saturation state, across all spatial surveys over the sampling season (see text), overlaid on map of vegetation cover. An effect size of 0.5 means that, compared to the mean across the pond, oxygen increases at a given sample location were 50% less variable over the sampling season. More vegetated areas of the pond generally had greater variability in daily rates of increase, as well as larger daily increases (Table S2 in **Online Resource S3**).

Figure 6. Net to gross productivity ratios

The ratio of dissolved oxygen-based net ecosystem metabolism (NEM) to gross oxygen production derived from either a dissolved oxygen diel mass balance or the triple oxygen isotope method (GOP_{O2} or GOP_{TOI}). The two leftmost boxes represent the range of observed 24 hour NEM/GOP ratios (including night and day), while the two rightmost boxes represent daytime NEM/GOP ratios (dawn to dusk). A value of zero (thick horizontal line) indicates no net consumption or storage of primary production in the system, while a negative value indicates net heterotrophy. Box heights represent the interquartile ranges of data, upper box whiskers encompass maximum observed ratios, lower box whiskers are 1.5 times the interquartile length, and individual points represent observations more negative than the lower whisker, encompassing the bottom 4-8% of the data. Thin horizontal lines within the boxes indicate the median of observations, and notch height represents the 95% confidence interval in the median—

overlapping notches indicate medians are not significantly different for NEM/GOP_{O2} and NEM/GOP_{TOI}.

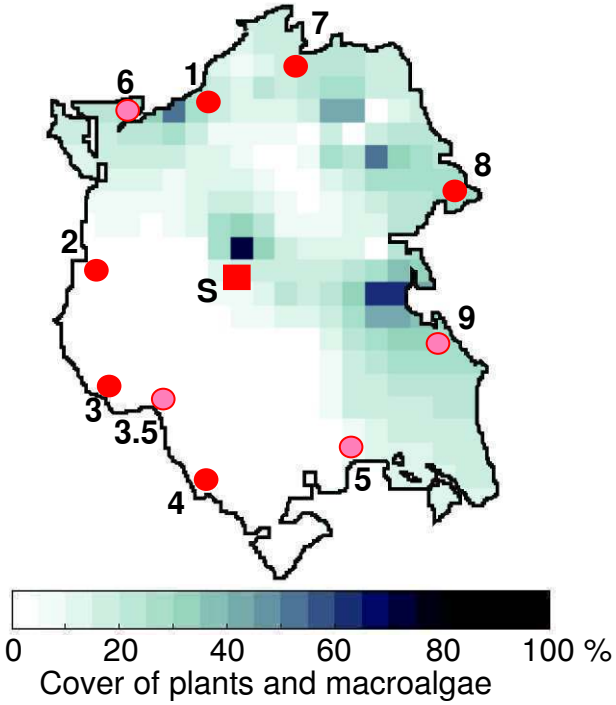
7
6
1
8
2
S
9
3
3.5
5
4
0
20
40
60
80
100 %
Cover of plants and macroalgae

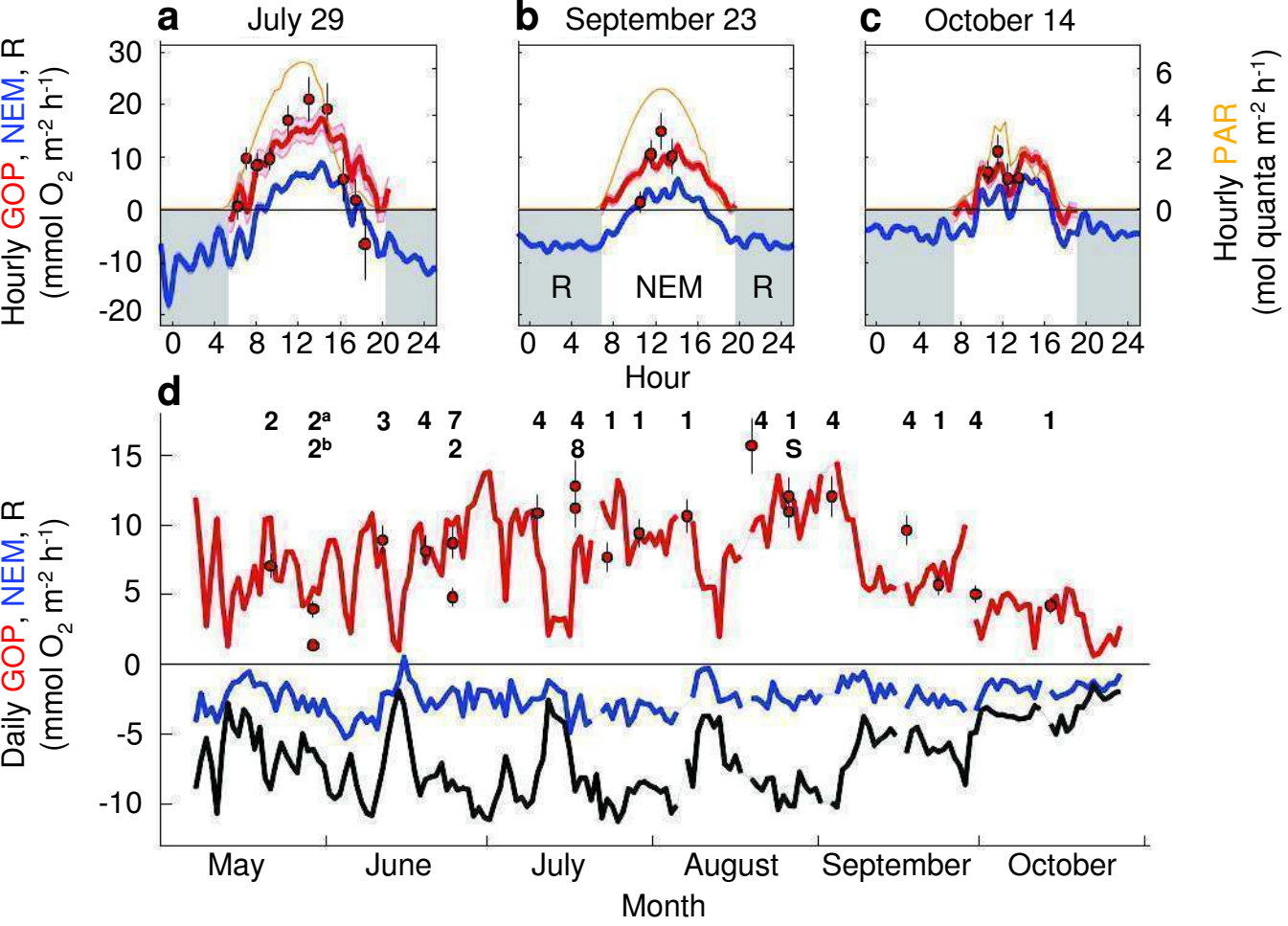
a
July 29
b
September 23
c
October 14
Hourly GOP, NEM, R
(mmol O2 m-2 h-1)
Hourly PAR
(mol quanta m-2 h-1)
R
NEM
R
Hour
d
2
2a
2b
3
4
7
2
4
4
8
1
1
1
4
1
S
4
4
1
4
1
Daily GOP, NEM, R
(mmol O2 m-2 h-1)
May
June
July
August
September
October
Month

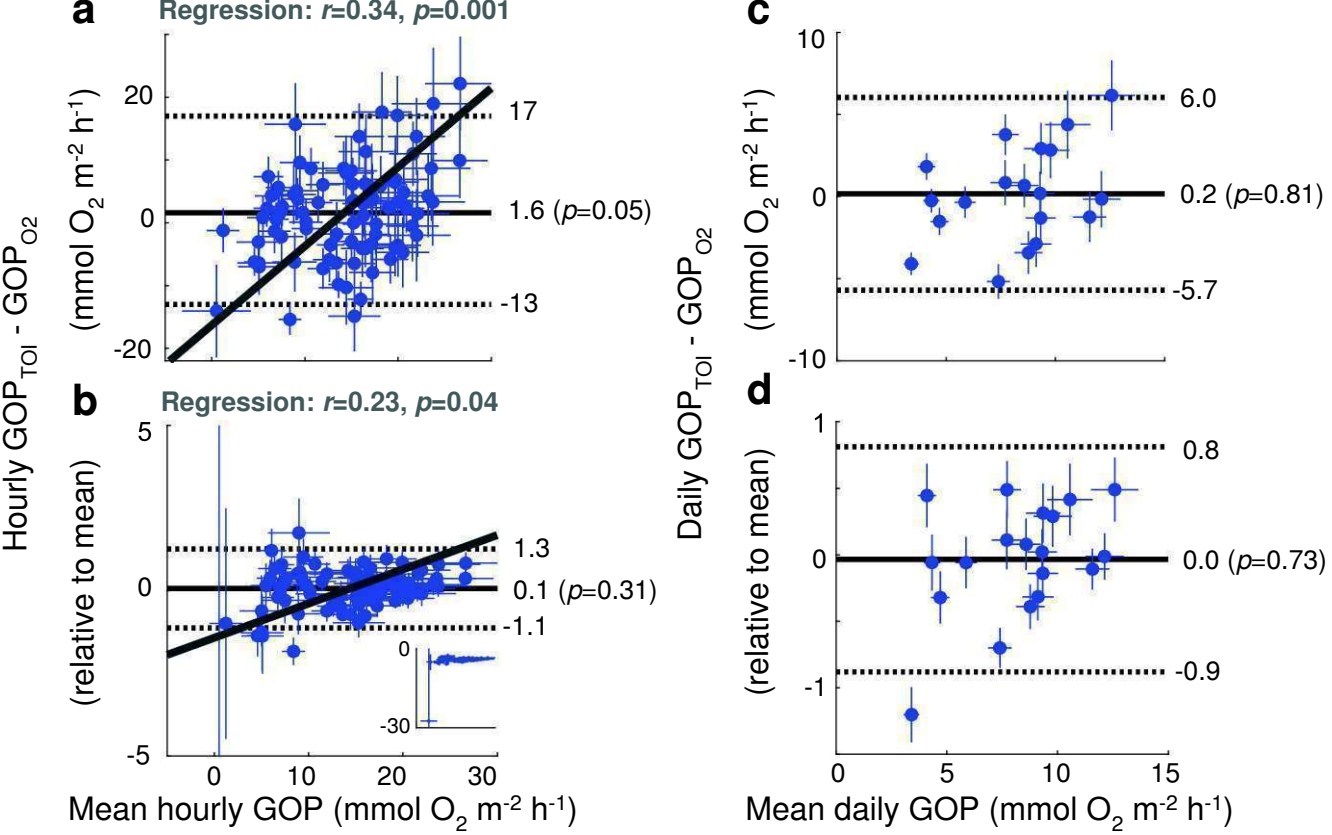
a
Regression: r=0.34, p=0.001
20
0
-20
17
1.6 (p=0.05)
-13
b
Regression: r=0.23, p=0.04
5
0
-5
1.3
0.1 (p=0.31)
-1.1
0
-30
0
10
20
30
Mean hourly GOP (mmol O2 m-2 h-1)
Hourly GOPTOI - GOPO2
(mmol O2 m-2 h-1)
(relative to mean)
c
10
0
-10
6.0
0.2 (p=0.81)
-5.7
d
1
0
-1
0.8
0.0 (p=0.73)
-0.9
0
5
10
15
Mean daily GOP (mmol O2 m-2 h-1)
Daily GOPTOI - GOPO2
(mmol O2 m-2 h-1)
(relative to mean)

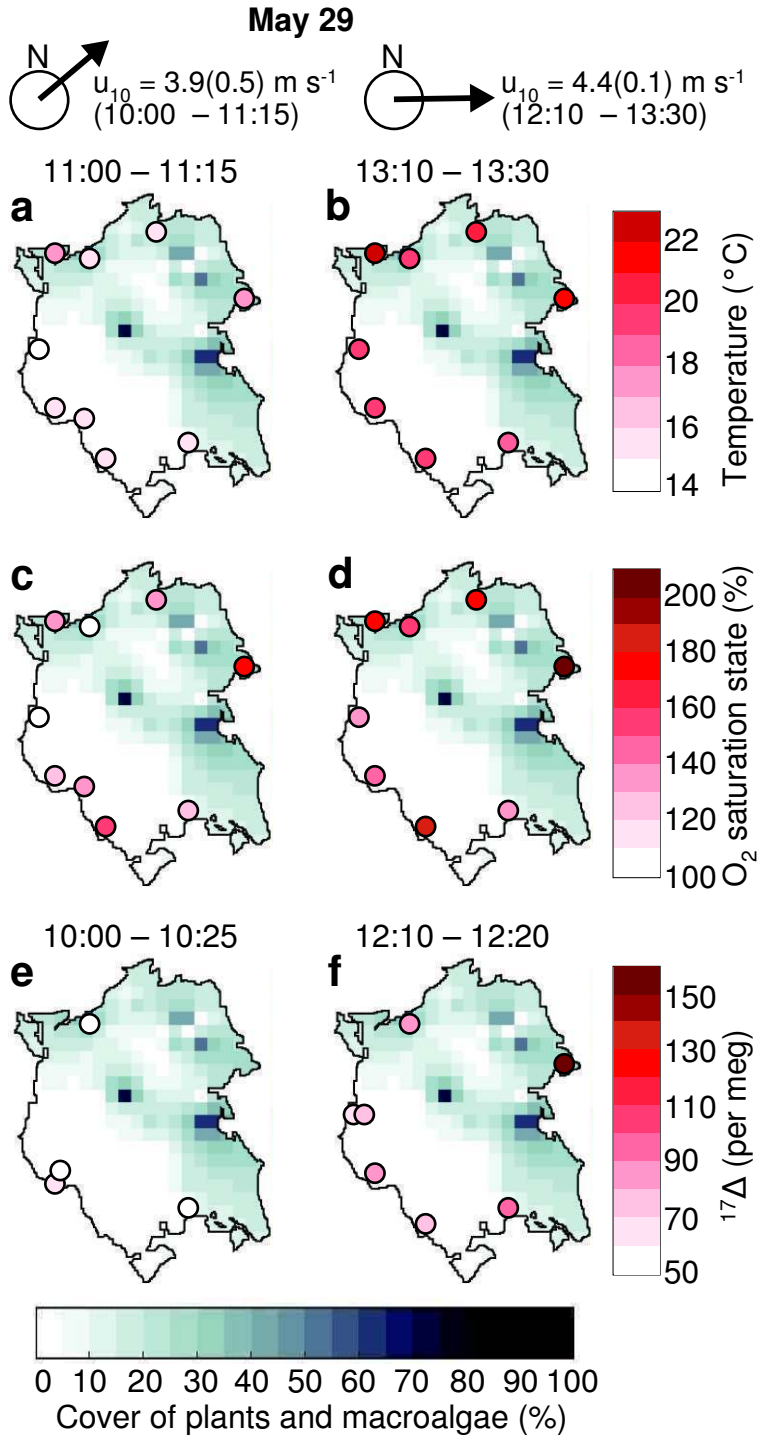
May 29
N
u_{10} = 3.9(0.5) m s^{-1}
(10:00 – 11:15)
N
u_{10} = 4.4(0.1) m s^{-1}
(12:10 – 13:30)
11:00 – 11:15
13:10 – 13:30
a
b
22
20
18
16
14
Temperature (°C)
c
d
200
180
160
140
120
100
O_2 saturation state (%)
10:00 – 10:25
12:10 – 12:20
e
f
150
130
110
90
70
50
$^{17}\Delta$ (per meg)
0 10 20 30 40 50 60 70 80 90 100
Cover of plants and macroalgae (%)

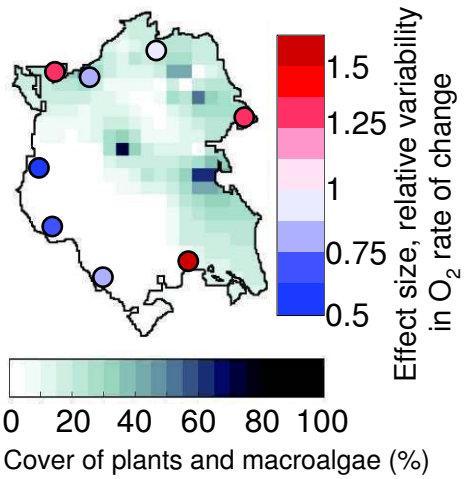
1.5
1.25
1
0.75
0.5
Effect size, relative variability in O_2 rate of change
0
20
40
60
80
100
Cover of plants and macroalgae (%)

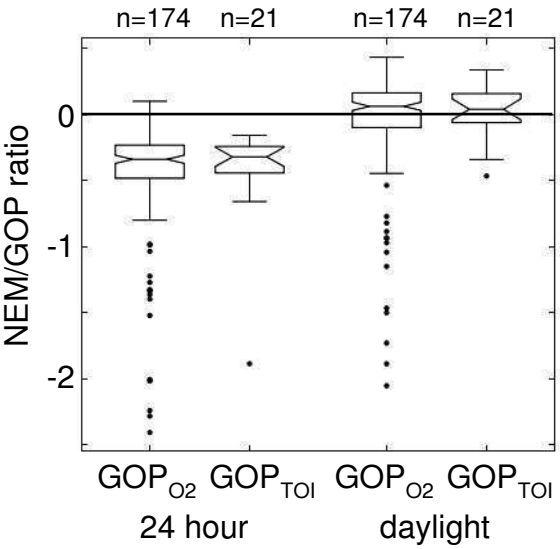
n=174
n=21
n=174
n=21
0
-1
-2
NEM/GOP ratio
GOP$_{O2}$
GOP$_{TOI}$
GOP$_{O2}$
GOP$_{TOI}$
24 hour
daylight

Dissolved oxygen and triple oxygen isotope measurements provide different insights into gross oxygen production in a shallow salt marsh pond

Estuaries and Coasts

Evan M. Howard*, Amanda C. Spivak, Jennifer S. Karolewski, Kelsey M. Gosselin, Zoe O. Sandwith, Cara C. Manning, Rachel H. R. Stanley

*Corresponding author: ehoward2@uw.edu, School of Oceanography, University of Washington, Seattle, WA, USA

Online Resource S1

Details of light-dependent processes with respect to divergence of gross oxygen production derived from a dissolved oxygen diel mass balance (GOP_{O2}) and the triple oxygen isotope method (GOP_{TOI}). In addition to references that also appear in the main text, supplementary references are provided here in order to provide additional context about the effect of these processes on the molecular oxygen and isotopic mass balances and production rates. References included here but not in the main text are not essential to the analysis or discussion presented in this work. Additionally, this supplement includes methodological details regarding data processing and analytical methods and two supporting figures.

Effects of light-dependent processes on GOP

Light-dependent O_2 consumption has been attributed to several processes in prior work, including photoreduction, photorespiration, direct light-stimulated mitochondrial respiration in autotrophs and resulting indirect stimulation of respiration in heterotrophs, and oxidation of reduced compounds in sediments.

Photoreduction, or the Mehler reaction, reduces O_2 to water at photosystem I (PSI), and can be a major oxygen uptake flux for autotrophs in the light, consuming as much O_2 from surrounding waters as 10-75% of photosystem II (PSII) O_2 output (Milligan et al. 2007, Halsey et al. 2010, Roberty et al. 2014). In eukaryotes, photoreduction is balanced by production, with no net O_2 consumption at the ecosystem level (Falkowski and Raven 1997), though some nitrogen fixing cyanobacteria may photoreduce without concurrent production of O_2 in order to maintain anoxic microenvironments (Milligan et al. 2007). In the absence of substantial nitrogen fixation, GOP_{O2} should not include photoreductive consumption of photosynthetic O_2. In contrast, GOP_{TOI} includes all PSII O_2 production regardless of compensating photoreductive consumption. Photoreduction appears to largely consume dissolved O_2 isotopically similar to that dissolved in the surrounding water (Kana 1990, Bender et al. 1999), and the relative isotope fractionations of this process differ from those of mitochondrial respiration (λ; Helman et al. 2005). Thus the triple oxygen isotopic mass balance must explicitly account for the removal of O_2 during the Mehler reaction if this process is significant (Equation 3d in main text). Without including this term GOP_{TOI} will be overestimated relative to GOP_{O2}. The isotopic fractionation factors for photoreduction (and their rratio between the triple oxygen isotopes) differ between eukaryotes and cyanobacteria, reflecting different cellular pathways (Helman et al. 2005, Latifi et al. 2008). Based on the single study of triple oxygen isotope systematics of photoreduction (Helman et al. 2005), the net result in eukaryotes is that the relative effect on GOP_{TOI} is only around half that of the proportion of photosynthetic O_2 consumed by photoreduction (10% of photosynthetic production consumed by photoreduction results in an ~4% change in GOP_{TOI} for isotope ratios typical in this study), while in cyanobacteria the effect on GOP_{TOI} is approximately proportional to the photoreductive consumption of O_2 (10% of photosynthetic production consumed by photoreduction results in an ~9% change in GOP_{TOI} for isotope ratios in this study).

Photorespiration occurs when ribulose-1,5-bisphosphate carboxylase/oxygenase, RuBisCo, consumes O_2 instead of carbon dioxide, at high O_2 and low carbon dioxide partial pressures. In terrestrial C3 plants and some eukaryotic algae and cyanobacteria, a smaller fraction of photorespiratory O_2 consumption occurs via glycolate oxidation (Beardall 1989, Eisenhut et al. 2008, Curien et al. 2016, Davis et al. 2017), by way of either glycolate oxidase or glycolate dehydrogenase (the latter does not consume dissolved O_2 and thus does not affect GOP). Photorespiration is thought to be a significant process in seagrasses (Buapet et al. 2013), but it is unclear whether glycolate oxidation plays a role (Touchette and Burkholder 2000, Larkum et al. 2006). RuBisCo photorespiration does not affect GOP_{TOI} as the triple isotope fractionation effects are indistinguishable from mitochondrial respiration (Helman et al. 2005). Glycolate oxidation has a different pattern of isotopic discrimination (Helman et al. 2005), but marine algae and cyanobacteria have efficient carbon dioxide-concentrating mechanisms that are thought to inhibit photoinhibition under normal environmental conditions (Kaplan and Rheinhold 1999). Thus, photorespiration would reduce GPP_{O2} because this net sink does not occur at night when R is determined, but it should have a limited effect on GPP_{TOI}.

Despite the potential O_2 fluxes associated with each process, both photoreduction and photorespiration are largely decoupled from organic carbon metabolism (Williams and del Giorgio 2005), and may primarily serve to remove excess electrons at the cellular level (Raven and Beardall 2005). In contrast, both direct (autotrophic) and indirect (heterotrophic) light-enhancement of mitochondrial respiration contribute to net O_2 fluxes and carbon metabolism at ecosystem scales (Grande et al. 1989, Pringault et al. 2009). Like photorespiration, light-enhanced mitochondrial respiration is not included in the calculation of GOP_{O2}, causing this rate to be lower than GOP_{TOI}.

Oxidation of sediment compounds may be directly or indirectly linked to carbon fluxes (e.g. through sulfur cycling; Luther et al. 1982, Wilbanks et al. 2014, Rao et al. 2016), with potentially different stoichiometry and delayed O_2 uptake compared to changes in the overlying water column (Fenchel and Glud 2000). While the apparent isotopic discrimination of O_2 in the overlying water appears to decrease with diffusion-limited O_2 supply to sediments (Brandes and Devol 1997), theory predicts no detectable difference in the triple isotope ratio of the fractionation factors (e.g., λ is unchanged; Li et al. 2019). Thus to the degree that sedimentary respiration varies over a day night cycle (e.g. because of stronger diffusive gradients from the water column), sedimentary uptake could decrease GOP_{O2} with little effect on GOP_{TOI}. However, dissolved O_2 that is completely produced and consumed within the sediments will not influence the isotopic characteristics of the bulk O_2 pool measured in the water column. At the extreme where all O_2 demand in excess of nighttime respiration rates is exactly matched by O_2 production within the sediments (all O_2 produced in sediments is consumed in the sediments and O_2 influx from the water column is unchanged compared to nighttime), then light-dependent sediment oxidation cannot influence the water column tracers. In this case neither GOP_{TOI} nor GOP_{O2} measured in the water column will include sedimentary productivity, and both rates will underestimate daytime productivity and diverge by less. In sandy sediment cores from 0.1-0.5 m depth in the Baltic Sea, between half and three-quarters of photosynthetic production in sediments was consumed within the sediments (Fenchel and Glud 2000).

Sensor deployment, calibration, and correction

In addition to individual laboratory sensor calibrations roughly every two weeks, from May 7 to July 8, 2014, four YSI™ sensor sondes were deployed sequentially and cross-calibrated with several hours of overlapping in situ data. One of these sensors was a potentiometric Clark-type O_2 electrode, while the

other three used fluorescence-based optode-type sensors. No sensor drift or offset between sondes was observed for temperature or O_2 saturation state.

Salinity from one sensor deployed during two periods in May evidenced both conductivity sensor drift and offsets compared to the other sensors. Offset and linear drift corrections were applied to this salinity data. Regardless, salinity effects on O_s concentrations derived from measured saturation state are small compared to temperature.

From July 8 through the end of the time series, a single YSI™Exo2 sonde was deployed sequentially, with data gaps of up to several hours while the instrument was cleaned and calibrated. Calibrations from before and after each deployment were compared, as well as the trends and magnitude of temperature, O_2 saturation state, and salinity on either side of the brief data gaps during maintenance. Each of these measures was consistent between calibrations and across gaps, with no evidence of measureable sensor drift over deployment periods or response offsets between deployments.

Vegetation cover interpolation and extrapolation

To fill gaps in the vegetation cover surveys, we used an image interpolation and extrapolation approach in which the data bounding each empty grid cell each acts as linear spring coefficients to "pull" the missing data towards their value (D'Errico 2012). The interpolated cell value is then the mean of the surrounding cells. In the absence of data in immediately adjacent cells, more distant data can contribute to the average, weighted inversely to their proximity to the location being interpolated. This approach leads to identical results to linear interpolation. However, values are extrapolated as a constant function (again weighted by proximity of the closest data). Thus extrapolation never exceeds the limits of observed data, unlike linear extrapolation; this prevents extrapolation to unrealistically high (or low) values in the absence of nearby data. We use vegetation cover qualitatively in this work, and thus make no attempt to constrain uncertainties associated with the extrapolation routine.

Triple oxygen isotope analytical methods

The samples and reference gas were balanced to a common voltage, resulting in similar pressures within the mass spectrometer. Isotopic ratios from O_2/Ar gas mixtures were corrected for the linear effects of Ar, trace amounts of dinitrogen, and the size of the sample—or more specifically the relative rates of sample and standard gas delivery to the mass spectrometer based on the differential compression of the bellows. The Ar calibration curve spanned $\delta(O_2/Ar)$ from roughly -700 to +100. Pond samples occasionally had higher $\delta(O_2/Ar)$, but the calibration curve was highly linear with small (~3%) relative errors in the slope fit. Each of the calibration curves, for each effect, were linear for $\delta^{17}O$, $\delta^{18}O$, and $^{17}\Delta$. All calibrations were performed during the study; the Ar calibrations change over monthly time scales and were performed every 2-4 weeks over the analysis period.

At approximately <50-65% O_2 saturation state, Ar matrix corrections were large compared to the oxygen isotope signals, introducing additional uncertainty in the triple oxygen isotope ratios. Thus, below 70% O_2 saturation ($[O_2]$ < 140-175 μmol kg^{-1}), Ar was manually separated from O_2 by using a gas chromatography column held in an isopropanol and dry ice slurry bath (-80°C). Once the Ar was eluted (observed using a quadrupole mass spectrometer attached to the carrier gas outflow), the bath was removed and the remaining oxygen passed through an additional liquid nitrogen trap in order to remove methane, and subsequently published normally. Methane was occasionally present in the samples and interfered with normal analysis on the isotope ratio mass spectrometer; methane concentrations were not

quantitatively determined, but were diagnosed using the quadrupole mass spectrometer used to monitor Ar elution. $^{17}\Delta$ and the oxygen isotope rations, reported in **Table S1** as $\delta^{17}O$ and $\delta^{18}O$, were then measured on the isotope ratio as with the samples with higher O_2 concentrations. Size and other corrections unrelated to Ar were applied similarly, but using separate calibration curves constructed using the Ar-free analysis method.

During methodological comparisons, we found no biases between the low-O_2 and regular method for triple oxygen isotope analysis at 70% or greater O_2 saturation state. This was true whether using water standards in this study, or environmental samples from nearby tidal creeks (Howard 2017). There was also no detectable difference in precision between replicates collected at night in this pond. The replicate precision, as standard deviation (and standard deviation thereof in parentheses), from samples processed using the low-O_2 method was 7(5) x10^{-2} per mil in $^{17}O/^{16}O$, 14(6) x10^{-2} per mil in $^{18}O/^{16}O$, and 4(3) per meg in $^{17}\Delta$. This was comparable to the standard method, in which replicate precision was 7(5) x10^{-2} per mil in $^{17}O/^{16}O$, 13(5) x10^{-2} per mil in $^{18}O/^{16}O$, and 5(6) per meg in $^{17}\Delta$; in either case this was equivalent to a relative error of 4% in $^{17}\Delta$. Overall these results suggest that the two methods are equivalent and the low-O_2 method is an acceptable substitution when the O_2/Ar is low enough to bias the standard method.

High precision measurement of $^{17}\Delta$ becomes more difficult as the amount of oxygen available for analysis in a sample decreases, and as oxygen isotopic ratios become less homogenous in the sampled environment. Analysis of these samples using the method above is impractical at $[O_2] < 50$ μmol kg^{-1}. No samples collected from the water column of this pond were below this threshold.

For all samples, regardless of whether or not Ar was removed, $^{17}\Delta$ was measured directly on the mass spectrometer more precisely than $\delta^{17}O$ and $\delta^{18}O$ individually. As $\delta^{18}O$ had relatively smaller corrections and greater precision than $\delta^{17}O$. Thus, for further calculations using the individual isotope rates we used measured $^{17}\Delta$ and $\delta^{18}O$ to recalculate a value of $\delta^{17}O$ for each sample that was internally consistent and preserved the $^{17}\Delta$ relationship between the three isotopes for the correct calculation of GOP_{TOI}. The difference between measured and calculated $\delta^{17}O$ is insignificant (-0.2(0.1)% relative error. However, using measured $\delta^{17}O$ and $\delta^{18}O$ directly to calculate $^{17}\Delta$ results in a mean relative difference in $^{17}\Delta$ of 4(4)% compared to the directly measured value; this constitutes a systematic difference in $^{17}\Delta$ of similar magnitude to the analytical uncertainty, and thus biases resulting GOP_{TOI} compared to the recalculated values used in this work.

Pressure baseline offsets between sample and standard gas have been proposed as a source of error in triple oxygen isotope analyses run on O_2/Ar mixtures when the sample and reference gas diverge in composition (Yeung et al. 2018). Because our samples run using the O_2/Ar method span a range of compositions, we checked for potential sensitivities to pressure baselines. However, we did not find any indication that they influenced our results. Aside from finding no difference between samples run using the O_2/Ar and O_2 only methods (for which we expect pressure baseline errors would be different), we applied a pressure baseline bias correction to our measured $^{17}\Delta$ as a function of $\delta^{18}O$ consistent with the sensitivities proposed in Yeung et al. (2018), between -4 and +4 per meg in $^{17}\Delta$ for each 1 per mil increase or decrease in $\delta^{18}O$. This led to either compression or expansion of the dynamic range in $^{17}\Delta$ and GOP_{TOI} over each day of sampling, decorrelating GOP_{TOI} form both GOP_{O2} and PAR. With either positive or negative sensitivities to pressure baselines, including such an effect resulted in GOP_{TOI} substantially less than GOP_{O2} over large portions of the day (at the beginning and end of the day at the one extreme, and in the middle of the day at the other). To the best of our knowledge there is no biological or physical mechanism that could support such a relationship in this setting, implying that uncorrected pressure baselines are not important factors in this dataset. Testing a range of slopes, pressure baseline effects must be at most $^{17}\Delta$ =~5 per meg at $\delta^{18}O$= -15 per mil before including post hoc corrections makes the statistical comparisons in this work less robust; this is similar to the evaluated random error in the measurements.

It may be that the linear calibrations to Ar and sample size may already adequately account for any pressure baseline effects on the mass spectrometer—both corrections can be of similar size to proposed pressure baseline effects. Such calibration and correction schemes are widely used for triple oxygen isotope analyses on O_2/Ar sample and reference mixtures in the oceanographic community. The equivalency of pressure baseline and Ar/size calibration schemes has not yet been rigorously demonstrated.

Finally, the choice of λ modifies Eq. 2, Eq. 3 and resulting $^{17}\Delta$ and GOP_{TOI}. While GOP_{TOI} can be sensitive to this definition, in this setting $0.518 \leq \lambda \leq 0.522$ leads to qualitatively similar results that do not alter our conclusions. For example, if $\lambda=0.522$, as suggested by Ash et al. (2020), GOP_{TOI} is generally reduced by 5-15%, and GOP_{TOI} is still elevated relative to GOP_{O2} at peak productivity. Hourly GOP from each method is slightly better correlated, while daily GOP rates become less correlated between the methods.

References

Ash, J.L., H. Hu, and Y. Yeung. 2020. What fractionates oxygen isotopes during respiration? Insights from multiple stable isotopologue measurements and theory. *ACS Earth Space Chem.* 4: 50-66. doi: 10.1021/acsearthspacechem.9b00230

Beardall, J. 1989. Photosynthesis and photorespiration in marine phytoplankton. *Aquat. Biol.* 34(1-3): 105-130. doi: 10.1016/0304-3770(89)90052-1

Bender, M., J. Orchardo, M-L. Dickson, R. Barber, and S. Lindley. 1999. In vitro O_2 fluxes compared with ^{14}C production and other rate terms during the JGOFS Equatorial Pacific experiment. *Deep Sea Res I* 46(4): 637-654. doi: 10.1016/S0967-0637(98)00080-6.

Brandes, J.A., and A.H. Devol. 1997. Isotopic fractionation of oxygen and nitrogen in coastalmarine sediments. *Geochmi. Cosmochim. Acta* 61(9): 1793-1801. doi: 10.1016/S0016-7037(97)00041-0

Curien, G., S. Flori, V. Villanova, L. Magneschi, C. Giustini, G. Forti, M. Matringe, D. Petroutsos, M. Kuntz, and G. Finazzi. 2016. The water to water cycles in microalgae. *Plant Cell Phys.* 57(7): 1354-1363. doi: 10.1093/pcp/pcw048

Davis, A., R., Abbriano, S.R. Smith, and M. Hildebrand. 2017. Clarification of photorespiratory processes and the role off malic enzyme in diatoms. *Protist* 168(1): 134-153. doi: doi.org/10.1016/j.protis.2016.10.005

D'Errico, J. 2012. inpaint_nans v.1.1. Matlab File Exchange. https://www.mathworks.com/matlabcentral/fileexchange/4551-inpaint_nans. Accessed 1 August 2017.

Eisenhut, M., W. Ruth, M. Haimovich, H. Bauwe, A. Kaplan, and M. Hagemann. 2008. The photorespiratory glycolate metabolism is essential for cyanobacteria and might have been coveyed endosymbiontically to plants. *Proc. Natl. Acad. Sci.* 105(44): 17199-17204. doi: 10.1073/pnas.0807043105

Falkowski, P.G., and J.A. Raven. 1997. *Aquatic photosynthesis*. Paris: Blackwell Science.

Fenchel, T., and R.N. Glud. 2000. Benthic primary production and O_2-CO_2 dynamics in a shallow-water sediment: Spatial and temporal heterogeneity. *Ophelia* 53(2): 159-171. doi: 10.1080/00785236.2000.10409446

Grande, K.D., J. Marra, C. Langdon, K. Heinemann, and M.L. Bender. 1989. Rates of respiration in the light measured in marine phytoplankton using an ^{18}O isotope-labeling technique. *J. Exper. Mar. Biol. Ecol.* 129(2): 95-120. doi: 10.1016/0022-0981(89)90050-6

Halsey, K.H., A.J. Milligan, and M.J. Behrenfeld. 2010. Physiological optimization underlies growth rate-independent chlorophyll-specific gross and net primary production. *Photosynth. Res.* 103(2): 125-137. doi: 10.1007/s11120-009-9526-z

Helman, Y., E. Barkan, D. Eisenstadt, and A. Kaplan. 2005. Fractionation of the three stable oxygen isotopes by oxygen-proucing and oxygen-consuming reactions in photosynthetic organisms. *Plant Physiol.* 138(4): 2292-2298. doi: 10.1104/pp.105.063768

Howard, E.M. 2017. *Ecosystem metabolism in salt marsh tidal creeks and ponds: Applying triple oxygen isotopes and other gas tracers to novel environments*. 69-70, 135-172. Woods Hole, MA: PhD thesis submitted to the Massachusetts Institute of Technology and the Woods Hole Oceanographic Institution. doi: 10.1575/1912/8654

Kana, T.M. 1990. Light-dependent oxygen cycling measured by an oxygen-18 isotope dilution technique. *Mar. Ecol. Prog. Ser.* 64: 293-300. doi: 10.3354/meps064293

Kaplan, A., and L. Reinhold. 1999. CO_2 concentrating mechanisms in photosynthetic microorganisms. *Ann. Rev. Plant Phys. Plant Molec. Biol.* 50: 539-570. doi: 10.1146/annurev.arplant.50.1.539

Larkum, A.W.D., E.A. Drew, and P.J. Ralph. 2006. Photosynthesis and metabolism in seagrasses at the cellular level. In *Seagrasses: Biology, ecology, and conservation*, eds. Larkum, Orth, and Duarte, 323-345. Dordrecht, Netherlands: Springer. doi: 10.1007/978-1-4020-2983-7_14

Raven, J.A., and J. Beardall. 2005. Respiration in aquatic photolithotrophs. In *Respiration in Aquatic Ecosystems*, eds. del Giorgio and Williams, 36-46. Oxford: Oxford U. Press.

Latifi, A., M. Ruiz, and C-C Zhang. 2009. Oxidative stress in cyanobacteria. *FEMS Microbiol. Rev.* 33(2): 258-278. doi: 10.1111/j.1574-6976.2008.00134.x

Li, B., L.Y. Yeung, H. Hu, and J.L. Ash. 2019. Kinetic and equilibrium fractionation of O_2 isotopologues during air-water gas transfer and implications for tracing oxygen cycling in the ocean. *Mar. Chem.* 210: 61-71. doi: 10.1016/j.marchem.2019.02.006

Luther III, G.W., A. Giblin, R.W. Howarth, and R.A. Ryans. 1982. Pyrtie and oxidized iron mineral phases formed from pyrite oxidation in salt marsh and estuarine sediments. *Geochim. Cosmochim. Acta* 46(12): 2665-2669. doi: 10.1016/0016-7037(82)90385-4

Milligan, A.J., I. Berman-Frank, Y. Gerchman, G.C. Dismukes, and P.G. Falkowski. 2007. Light-dependent oxygen consumption in nitrogen-fixing cyanobacteria plays a key role in nitrogenase protection. *J. Phycol.* 43(5): 845-852. doi: 10.1111/j.1529-8817.2007.00395.x

Pringault, O., S. Tesson, and E. Rochelle-Newall. 2009. Respiration in the light and bacterio-phytoplankton coupling in a coastal environment. *Microb. Ecol.* 57(2): 321-334. doi: 10.1007/s00248-008-9422-7

Rao, A., N. Risgaard-Petersen, and U. Neumeier. 2016. Electrogenic sulfur oxidation in a northern saltmarsh (St. Lawrence Estuary, Canada). *Canad. J. Microbiol.* 62(6): 530-537. doi: 10.1139/cjm-2015-0748

Raven, J.A., and J. Beardall. 2005. Respiration in aquatic photolithotrophs. In *Respiration in Aquatic Ecosystems*, eds. del Giorgio and Williams, 36-46. Oxford: Ocford U. Press.

Roberty, S., B. Bailleul, N. Berne, F. Franck, and P. Cardol. 2014. PSI Mehler reaction is the main alternative photosynthetic electron pathway in Symbiodinium sp., symbiotic dinoflagellates of cnidarians. *New Phytologist* 204(1): 81-91. doi: 10.1111/nph.12903

Touchette, B.W., and J.M. Burkholder. 2000. Overview of the physiological ecology of carbon metabolism in seagrasses. *J. Exper. Mar. Biol. Ecol.* 250(1-2): 169-205. doi: 10.1016/S0022-0981(00)00196-9

Wilbanks, E.G., U. Jaekel, V. Salman, P.T. Humphrey, J.A. Eisen, M.T. Facciotti, D.H. Buckley, S.H. Zinder, G.K. Druschel, D.A. Fike, and V.J. Orphan. 2014. Microscale sulfur cycling in the phototrophic pink berry consortia of the Sippewissett Salt Marsh. *Environ. Microbiol.* 16(11): 3398-3415. doi: 10.1111/1462-2920.12388

Williams, P.J. le B., and P.A. del Giorgio. Respiration in aquatic ecosystems: history and background. In *Respiration in aquatic ecosystems*, eds. del Giorgio and Williams, 1-17. Oxford: Oxford U. Press.

Yeung, L.Y., J.A. Hayles, H. Hu, J.L. Ash, and T. Sun. 2018. Scale distortion from pressure baseline as a source of inaccuracy in triple-isotope measurements. *Rap. Comm. Mass Spec.* 32(20): 1811-1821, doi: 10.1002/rcm.8247

Supporting figures

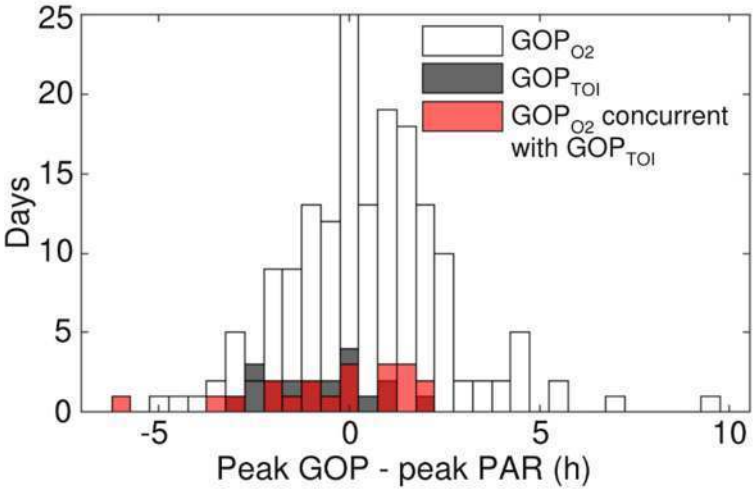

Figure S1. Time difference between daily peak in light and productivity

Histogram of the time difference between the maximum hourly gross oxygen production rate (GOP) and the maximum flux of photosynthetically active radiation (PAR). Counts are binned in 30 minute intervals centered on peak daily PAR. Dark red shading marks overlapping counts of GOP_{TOI} (black), and GOP_{O2} from only the days on which GOP_{TOI} was also measured (light red); thus, the histogram of GOP_{TOI} is shown by black and dark red counts, and that of GOP_{O2} from the same days by light red and dark red counts. The time of peak daily PAR varied with season and cloud cover over the time series. In general, large offsets in time between PAR and productivity were associated with low light or recent tidal flooding, both of which were low-productivity periods.

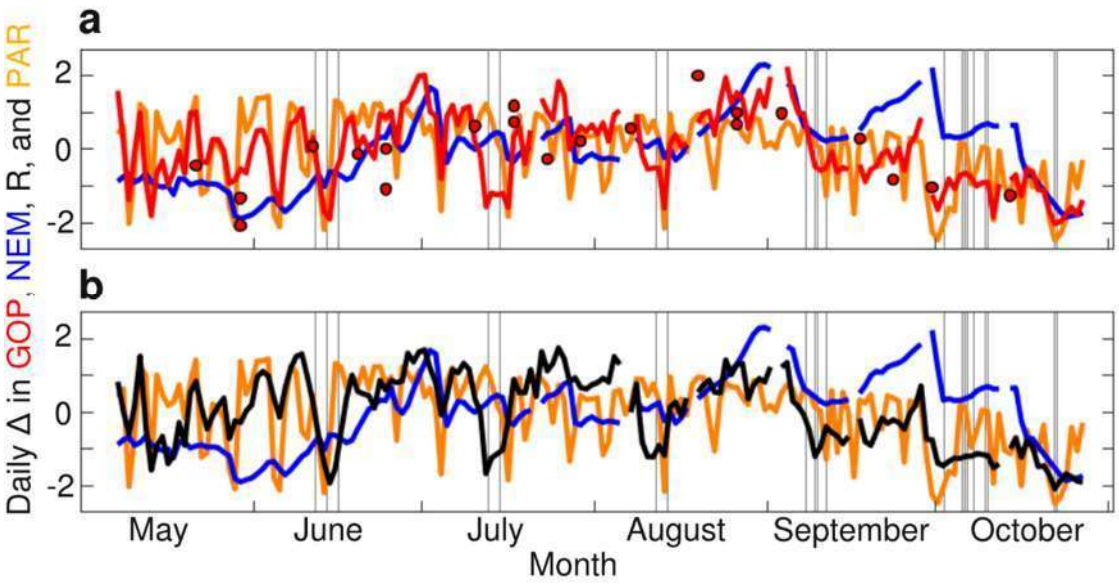

Figure S2. Time series anomalies of metabolic rates in relation to light and tidal stage

Standardized anomalies (Δ) are calculated as the value normalized to the time series mean and divided by the standard deviation over the time series (e.g., for variable x and observation i, $\Delta x_i=[x_i - \text{mean}(x)]/\text{standard deviation}(x)$). (**a**) Standardized anomalies of gross oxygen production (GOP_{O2}, red line, and GOP_{TOI}, red circles), net ecosystem metabolism (NEM, blue line) and photosynthetically active radiation flux (PAR, orange line). (**b**). Standardized anomalies of NEM, PAR, and dark respiration and sediment oxygen uptake, R (black line). Gray shading indicates periods during which tidal height was greater than 1.46 m relative to the North American Vertical Datum of 1988, resulting in flooding of the marsh platform and pond.

Dissolved oxygen and triple oxygen isotope measurements provide different insights into gross oxygen production in a shallow salt marsh pond

Estuaries and Coasts

Evan M. Howard*, Amanda C. Spivak, Jennifer S. Karolewski, Kelsey M. Gosselin, Zoe O. Sandwith, Cara C. Manning, Rachel H. R. Stanley

*Corresponding author: ehoward2@uw.edu, School of Oceanography, University of Washington, Seattle, WA, USA

Online Resource S2

Equations, constants, and derivation for calculation of gross oxygen production using triple oxygen isotopes incorporating a variety of physical and biological processes. References for definitions, values, and equations are provided; some of these references do not appear in the main text because the associated processes are not a focus of this work, but are included here for completeness when presenting the mass balance terms for a variety of processes which may affect the oxygen isotopic balances in natural environments. Additionally, an example calculation.

Equations

(1) $^{i}\mathrm{X} = (^{i}\mathrm{O}/^{16}\mathrm{O})_{\mathrm{sample}}/(^{i}\mathrm{O}/^{16}\mathrm{O})_{\mathrm{air}} = {}^{i}\delta + 1$ — i is heavy isotope

(2) $^{i}\mathrm{X}_{\mathrm{j}} = (^{i}\mathrm{O}/^{16}\mathrm{O})_{\mathrm{endmember}}/(^{i}\mathrm{O}/^{16}\mathrm{O})_{\mathrm{air}} = {}^{i}\delta_{\mathrm{j}} + 1$ — j is endmember

(3) $$^{i}\mathrm{A}_{\mathrm{j}} = \frac{^{i}\mathrm{X}_{\mathrm{j}}\ ^{i}\alpha_{e}\ ^{i}\alpha_{k}}{^{i}\mathrm{X}} - 1$$ — α_k (kinetic) and α_e (equilibrium), isotopic fractionation factors, if applicable

(4) $$^{17}\Delta = \left[\ln\left(^{17}\mathrm{X}\right) - \lambda \ln\left(^{18}\mathrm{X}\right)\right] \times 10^{6} \text{ per meg}$$ — Angert et al. 2003 definition

(5) $$h[\mathrm{O}_2]\frac{\partial}{\partial \mathrm{t}}\left(^{17}\Delta\right)$$ — Change in tracer with time

$$= \mathrm{GOP}\left(^{17}\mathrm{A}_{\mathrm{P}} - \lambda\, ^{18}\mathrm{A}_{\mathrm{P}}\right)$$ — Gross oxygen production

$$+ \mathrm{k}_{\mathrm{O2}}[\mathrm{O}_2]_{\mathrm{sat}}\left(^{17}\mathrm{A}_{\mathrm{G}} - \lambda\, ^{18}\mathrm{A}_{\mathrm{G}}\right)\ldots - \mathrm{k}_{\mathrm{O2}}[\mathrm{O}_2]\left(\left(^{17}\alpha_k - 1\right) - \lambda\left(^{18}\alpha_k - 1\right)\right)$$ — Air-water gas exchange[1]

$$+ \left(\frac{\partial h}{\partial t} + \frac{\partial \kappa_z}{\partial z}\right)[\mathrm{O}_2]_z\left(^{17}\mathrm{A}_{\mathrm{V}} - \lambda\, ^{18}\mathrm{A}_{\mathrm{V}}\right)$$ — Vertical entrainment & mixing[2]

$$+ h\left(\frac{\partial}{\partial x}\left(\kappa_x \frac{\partial([\mathrm{O}_2]\,^{17}\mathrm{X})}{\partial x}\right)\frac{1}{^{17}\mathrm{X}} - \lambda\left(\frac{\partial}{\partial x}\left(\kappa_x \frac{\partial([\mathrm{O}_2]\,^{18}\mathrm{X})}{\partial x}\right)\frac{1}{^{18}\mathrm{X}}\right)\right) - h(1-\lambda)\left(\frac{\partial}{\partial x}\left(\kappa_x \frac{\partial[\mathrm{O}_2]}{\partial x}\right)\right)$$ — Lateral mixing

$$+ h\left(\frac{\partial}{\partial x}\left(\mathrm{u}_x[\mathrm{O}_2]\,^{17}\mathrm{X}\right)\frac{1}{^{17}\mathrm{X}} - \lambda\left(\frac{\partial}{\partial x}\left(\mathrm{u}_x[\mathrm{O}_2]\,^{18}\mathrm{X}\right)\frac{1}{^{18}\mathrm{X}}\right)\right) - h(1-\lambda)\left(\frac{\partial}{\partial x}\left(\mathrm{u}_x[\mathrm{O}_2]\right)\right)$$ — Lateral transport

$$+ F_{b,ex}\chi_{O2,b}\left({}^{17}A_B - \lambda\,{}^{18}A_B\right) - F_{b,ex}[O_2]\left[\left({}^{17}\alpha_k - 1\right) - \lambda\left({}^{18}\alpha_k - 1\right)\right]$$ Bubble exchange or ebullition[3]

$$+ F_{b,inj}\chi_{O2,b}\left[\left(\frac{X_a}{{}^{17}X} - 1\right) - \lambda\left(\frac{X_a}{{}^{18}X} - 1\right)\right]$$ Bubble injection[4]

$$- LD\left({}^{17}A_{LD} - \lambda\,{}^{18}A_{LD}\right)$$ Light-dependent process[5]

Notes

[1] Equivalent to Hamme et al. 2012, Li et al. 2019

[2] Equivalent to Nicholson et al. 2014, Howard et al. 2017

[3] Bubble composition depends on source (air versus ebullition from sediments or water column, subsequent equilibration). $F_{b,ex}$ depends on total bubble volume as well as bubble size-dependent water-bubble transfer rates, and bubble to water transfer must include molar volume conversion (e.g. $+F_{b,ex}$ does not have same units as $-F_{b,ex}$ as written).

[4] Equivalent to Kaiser 2011 if bubble injection flux has units of mmol air m^{-2} h^{-1}.

[5] Photoreduction predominantly consumes O_2 which is isotopically similar to that of that dissolved in the surrounding water (Kana et al. 1990, Bender et al 1999), and the term simplifies to that in Equation 3d of the main text. Other light-dependent processes might consume some portion of photosynthetic O_2 (with isotopic composition ${}^{i}X_w{}^{i}\alpha_{k,P}$).

Constants and values used in this work	**Source**
Isotopes	
${}^{i}X_a = {}^{i}X$ air = 1 when isotope ratios are referenced to air	
${}^{i}X_w = {}^{i}X$ in substrate water ${}^{17}X_w$=0.98689 to 0.98759, ${}^{18}X_w$=0.97438 to 0.97570	Manning et al. 2017
${}^{i}X = {}^{i}X$ of dissolved O_2 in sample ${}^{17}X$=0.99276 to 01.00362, ${}^{18}X$=0.98568 to 1.00665	Measured
${}^{i}X_z = {}^{i}X$ of dissolved O_2 in sample at depth below mixed layer	
${}^{i}X_b = {}^{i}X$ of dissolved O_2 inside bubble	
$\lambda = ({}^{17}\alpha_{k,respiration}\text{-}1)/({}^{18}\alpha_{k,respiration}\text{-}1) = 0.5179(0.0006)$	Luz and Barkan (2005)
$A_P({}^{i}X_w, {}^{i}\alpha_{k,P})$ ${}^{17}\alpha_{k,P}$=1.00025 to 1.00379; ${}^{18}\alpha_{k,P}$=1.00047 to 1.00704 for cyanobacteria, diatoms, and green algae	Helman et al. (2005), Eisenstadt et al. (2010), Luz and Barkan (2011)
$A_G({}^{i}X_a, {}^{i}\alpha_{e,G}\,{}^{i}\alpha_{k,G})$ ${}^{17}\alpha_{e,G}$=1.00035 to 1.00042 , ${}^{18}\alpha_{e,G}$=1.00067 to 1.00080 ${}^{17}\alpha_{k,G}$=0.9989, ${}^{18}\alpha_{k,G}$=0.9978	Benson and Krause (1980, 1984), Manning et al. 2017, Li et al. (2019)
$A_V({}^{i}X_z)$	
$A_B({}^{i}X_{b,}, {}^{i}\alpha_{e,G}\,{}^{i}\alpha_{k,G})$	
$A_{LD}({}^{i}X, {}^{i}\alpha_{k,LD})$	See **Online Resource S2**

Concentrations

$[O_2]$ = molar concentration of dissolved O_2

$[O_2]_{sat}$ = saturation concentration at air-water equilibrium Garcia and Gordon (1992, 1993)

$[O_2]_z$ = concentration in sample at depth below mixed layer

$[O_2]_b$ = concentration in equilibrium with bubble composition

$\chi_{O2,b}$ = mole fraction of O_2 in bubble

Dimensions and rates

h = depth of vertically well-mixed water parcel being considered

t = time

x = horizontal distance (for one dimensional lateral mixing or flow)

z = vertical distance (for vertical mixing or flow)

k_{O2} = air water gas transfer coefficient for O_2 Vachon and Prairie (2013)

κ_z = vertical diffusivity

κ_x = horizontal diffusivity

u_x = horizontal velocity

GOP = gross oxygen production

$F_{b,ex}$ = bubble exchange flux (partial dissolution of bubble)

$F_{b,inj}$ = bubble injection flux (complete dissolution of bubble)

LD = light dependent process of interest

Derivation

This derivation generally follows the approach of Prokopenko et al. 2011. Because the rates of change of oxygen concentration and the well-mixed surface layer depth are substituted into the isotopic equation, these terms are implicitly included in the final equation for instantaneous rates. When rates are assessed over discrete time intervals between two samples (times i:i+1), we set *h*, $[O_2]$, and transfer terms equal to the mean value between sample points (leading to n-1 rates). Alternatively, centered rates of change and processes based on preceding through following sample times (i-1:i+1) could be used and rates solved for conditions at the time of sampling (leading to n-2 rates).

Non-steady state production, gas exchange, and vertical entrainment and mixing

O_2 mass balance

1a. $\frac{\partial}{\partial t}(h[O_2]) = \mathrm{GOP} - \mathrm{R} + k_{O2}([O_2]_{sat} - [O_2]) + \frac{\partial h}{\partial t}[O_2]_z + \frac{\kappa_z}{\partial z}([O_2]_z - [O_2])$

1b. $\frac{\partial h}{\partial t}[\mathrm{O_2}] + h\frac{\partial[\mathrm{O_2}]}{\partial \mathrm{t}} = \mathrm{GOP} - \mathrm{R} + \mathrm{k_{O2}}([\mathrm{O_2}]_{\mathrm{sat}} - [\mathrm{O_2}]) + \frac{\partial h}{\partial t}[\mathrm{O_2}]_z + \frac{\kappa_z}{\partial z}([\mathrm{O_2}]_z - [\mathrm{O_2}])$

1c. $h\frac{\partial[\mathrm{O_2}]}{\partial \mathrm{t}} = \mathrm{GOP} - \mathrm{R} + \mathrm{k_{O2}}([\mathrm{O_2}]_{\mathrm{sat}} - [\mathrm{O_2}]) + \frac{\partial h}{\partial t}([\mathrm{O_2}]_z - [\mathrm{O_2}]) + \frac{\kappa_z}{\partial z}([\mathrm{O_2}]_z - [\mathrm{O_2}])$

1d. $h\frac{\partial[\mathrm{O_2}]}{\partial \mathrm{t}} = \mathrm{GOP} - \mathrm{R} + \mathrm{k_{O2}}([\mathrm{O_2}]_{\mathrm{sat}} - [\mathrm{O_2}]) + \left(\frac{\partial h}{\partial t} + \frac{\kappa_z}{\partial z}\right)([\mathrm{O_2}]_z - [\mathrm{O_2}])$

$^{i}O/^{16}O$ isotopic balance

2a. $\frac{\partial}{\partial t}\left(h[\mathrm{O_2}]\ {}^{i}\mathrm{X}\right) = \mathrm{GOP}\ {}^{i}\mathrm{X}_w\ {}^{i}\alpha_{k,P} - \mathrm{R}\ {}^{i}\mathrm{X}\ {}^{i}\alpha_{k,respiration}$

$+\ \mathrm{k_{O2}}\left([\mathrm{O_2}]_{\mathrm{sat}}\ {}^{i}\mathrm{X}_a\ {}^{i}\alpha_{e,G}\ {}^{i}\alpha_{k,G} - [\mathrm{O_2}]\ {}^{i}\mathrm{X}\ {}^{i}\alpha_{k,G}\right)$

$+\frac{\partial h}{\partial t}[\mathrm{O_2}]_z\ {}^{i}\mathrm{X}_z + \frac{\kappa_z}{\partial z}\left([\mathrm{O_2}]_z\ {}^{i}\mathrm{X}_z - [\mathrm{O_2}]\ {}^{i}\mathrm{X}\right)$

2b. $\frac{\partial h}{\partial t}[\mathrm{O_2}]\ {}^{i}\mathrm{X} + h\frac{\partial\left([\mathrm{O_2}]\ {}^{i}\mathrm{X}\right)}{\partial \mathrm{t}} = \cdots$

2c. $h\frac{\partial\left([\mathrm{O_2}]\ {}^{i}\mathrm{X}\right)}{\partial \mathrm{t}} = \mathrm{GOP}\ {}^{i}\mathrm{X}_w\ {}^{i}\alpha_{k,P} - \mathrm{R}\ {}^{i}\mathrm{X}\ {}^{i}\alpha_{k,res.}$

$+\ \mathrm{k_{O2}}\left([\mathrm{O_2}]_{\mathrm{sat}}\ {}^{i}\mathrm{X}_a\ {}^{i}\alpha_{e,G}\ {}^{i}\alpha_{k,G} - [\mathrm{O_2}]\ {}^{i}\mathrm{X}\ {}^{i}\alpha_{k,G}\right)$

$+\left(\frac{\partial h}{\partial t} + \frac{\kappa_z}{\partial z}\right)\left([\mathrm{O_2}]_z\ {}^{i}\mathrm{X}_z - [\mathrm{O_2}]\ {}^{i}\mathrm{X}\right)$

2d. $h\ {}^{i}\mathrm{X}\frac{\partial[\mathrm{O_2}]}{\partial \mathrm{t}} + h[\mathrm{O_2}]\frac{\partial\ {}^{i}\mathrm{X}}{\partial \mathrm{t}} = \cdots$

Substitute 1 into 2, divide by ^{i}X, and simplify with definition of $^{i}A_j$

3a. $\quad {}^{i}\mathrm{X}\left(\mathrm{GOP} - \mathrm{R} + \mathrm{k_{O2}}([\mathrm{O_2}]_{\mathrm{sat}} - [\mathrm{O_2}]) + \left(\frac{\partial h}{\partial t} + \frac{\kappa_z}{\partial z}\right)([\mathrm{O_2}]_z - [\mathrm{O_2}])\right) + h[\mathrm{O_2}]\frac{\partial\ {}^{i}\mathrm{X}}{\partial \mathrm{t}}$

$= \mathrm{GOP}\ {}^{i}\mathrm{X}_w\ {}^{i}\alpha_{k,P} - \mathrm{R}\ {}^{i}\mathrm{X}\ {}^{i}\alpha_{k,res.}$

$+\ \mathrm{k_{O2}}\left([\mathrm{O_2}]_{\mathrm{sat}}\ {}^{i}\mathrm{X}_a\ {}^{i}\alpha_{e,G}\ {}^{i}\alpha_{k,G} - [\mathrm{O_2}]\ {}^{i}\mathrm{X}\ {}^{i}\alpha_{k,G}\right)$

$+\left(\frac{\partial h}{\partial t} + \frac{\kappa_z}{\partial z}\right)\left([\mathrm{O_2}]_z\ {}^{i}\mathrm{X}_z - [\mathrm{O_2}]\ {}^{i}\mathrm{X}\right)$

3b. $\mathrm{GOP} - \mathrm{R} + \mathrm{k_{O2}}([\mathrm{O_2}]_{\mathrm{sat}} - [\mathrm{O_2}]) + \left(\frac{\partial h}{\partial t} + \frac{\kappa_z}{\partial z}\right)([\mathrm{O_2}]_z - [\mathrm{O_2}]) + h[\mathrm{O_2}]\frac{\partial\ {}^{i}\mathrm{X}}{\partial \mathrm{t}}\frac{1}{{}^{i}\mathrm{X}}$

$= \mathrm{GOP}\ {}^{i}\mathrm{X}_w\ {}^{i}\alpha_{k,P}\frac{1}{{}^{i}\mathrm{X}} - \mathrm{R}\ {}^{i}\alpha_{k,res.}$

$+\ \mathrm{k_{O2}}\left([\mathrm{O_2}]_{\mathrm{sat}}\ {}^{i}\mathrm{X}_a\ {}^{i}\alpha_{e,G}\ {}^{i}\alpha_{k,G}\frac{1}{{}^{i}\mathrm{X}} - [\mathrm{O_2}]\ {}^{i}\alpha_{k,G}\right)$

$$+\left(\frac{\partial h}{\partial t}+\frac{\kappa_z}{\partial z}\right)\left([\mathrm{O_2}]_\mathrm{z}\ {}^{i}\mathrm{X}_z\frac{1}{{}^{i}\mathrm{X}}-[\mathrm{O_2}]\right)$$

3c. $$h[\mathrm{O_2}]\frac{\partial\ {}^{i}\mathrm{X}}{\partial \mathrm{t}}\frac{1}{{}^{i}\mathrm{X}}=\ \mathrm{GOP}\left(\ {}^{i}\mathrm{X}_w\ {}^{i}\alpha_{k,P}\frac{1}{{}^{i}\mathrm{X}}-1\right)-\ \mathrm{R}(\ {}^{i}\alpha_{k,res.}-1)$$

$$+\ \mathrm{k_{O2}}\left([\mathrm{O_2}]_\mathrm{sat}\left(\ {}^{i}\mathrm{X}_a\ {}^{i}\alpha_{e,G}\ {}^{i}\alpha_{k,G}\frac{1}{{}^{i}\mathrm{X}}-1\right)-[\mathrm{O_2}](\ {}^{i}\alpha_{k,G}-1)\right)$$

$$+\left(\frac{\partial h}{\partial t}+\frac{\kappa_z}{\partial z}\right)\left([\mathrm{O_2}]_\mathrm{z}\left(\ {}^{i}\mathrm{X}_z\frac{1}{{}^{i}\mathrm{X}}-1\right)\right)$$

3d. $$h[\mathrm{O_2}]\frac{\partial\ {}^{i}\mathrm{X}}{\partial \mathrm{t}}\frac{1}{{}^{i}\mathrm{X}}=\mathrm{GOP}(\ {}^{i}\mathrm{A_P})-\ \mathrm{R}(\ {}^{i}\alpha_{k,res.}-1)$$

$$+\mathrm{k_{O2}}\left([\mathrm{O_2}]_\mathrm{sat}\ {}^{i}\mathrm{A_G}-[\mathrm{O_2}](\ {}^{i}\alpha_{k,G}-1)\right)$$

$$+\left(\frac{\partial h}{\partial t}+\frac{\kappa_z}{\partial z}\right)([\mathrm{O_2}]_\mathrm{z}\ {}^{i}\mathrm{A}_z)$$

Solve for triple isotope systematics in terms of $^{17}\Delta$, using definitions of $^{17}\Delta$ and λ

4a. $$h[\mathrm{O_2}]\frac{\partial {}^{17}\mathrm{X}}{\partial \mathrm{t}}\frac{1}{{}^{17}\mathrm{X}}=h[\mathrm{O_2}]\frac{\partial\ln({}^{17}\mathrm{X})}{\partial \mathrm{t}}\ \ \&\ \ h[\mathrm{O_2}]\frac{\partial {}^{18}\mathrm{X}}{\partial \mathrm{t}}\frac{1}{{}^{18}\mathrm{X}}=h[\mathrm{O_2}]\frac{\partial\ln({}^{18}\mathrm{X})}{\partial \mathrm{t}}$$

4b. $$h[\mathrm{O_2}]\frac{\partial {}^{17}\Delta}{\partial \mathrm{t}}=\ \mathrm{GOP}\left({}^{17}\mathrm{A_P}-\lambda\,{}^{18}\mathrm{A_P}\right)$$

$$+\ \mathrm{k_{O2}}[\mathrm{O_2}]_\mathrm{sat}\left({}^{17}\mathrm{A_G}-\lambda\,{}^{17}\mathrm{A_G}\right)-\ \mathrm{k_{O2}}[\mathrm{O_2}]\left(\left({}^{17}\alpha_k-1\right)-\lambda\left({}^{18}\alpha_k-1\right)\right)$$

$$+\left(\frac{\partial h}{\partial t}+\frac{\kappa_z}{\partial z}\right)[\mathrm{O_2}]_\mathrm{z}\left({}^{17}\mathrm{A}_z-\lambda\,{}^{18}\mathrm{A}_z\right)$$

Lateral mixing and advection

1. $$\frac{\partial}{\partial t}(h[\mathrm{O_2}])=\cdots+h\frac{\partial}{\partial x}\left(\kappa_x\frac{\partial[\mathrm{O_2}]}{\partial x}\right)+h\frac{\partial}{\partial x}(\mathrm{u}_x[\mathrm{O_2}])$$

2a. $$\frac{\partial}{\partial t}\left(h[\mathrm{O_2}]\ {}^{i}\mathrm{X}\right)=\cdots+h\frac{\partial}{\partial x}\left(\kappa_x\frac{\partial\left([\mathrm{O_2}]\ {}^{i}\mathrm{X}\right)}{\partial x}\right)+h\frac{\partial}{\partial x}\left(\mathrm{u}_x[\mathrm{O_2}]\ {}^{i}\mathrm{X}\right)$$

2b. $$h\ {}^{i}\mathrm{X}\frac{\partial}{\partial t}([\mathrm{O_2}])+h[\mathrm{O_2}]\frac{\partial}{\partial t}(\ {}^{i}\mathrm{X})=\cdots+h\frac{\partial}{\partial x}\left(\kappa_x\frac{\partial\left([\mathrm{O_2}]\ {}^{i}\mathrm{X}\right)}{\partial x}\right)+h\frac{\partial}{\partial x}\left(\mathrm{u}_x[\mathrm{O_2}]\ {}^{i}\mathrm{X}\right)$$

3a. $$h\ {}^{i}\mathrm{X}\left(\ldots+h\frac{\partial}{\partial x}\left(\kappa_x\frac{\partial[\mathrm{O_2}]}{\partial x}\right)+h\frac{\partial}{\partial x}(\mathrm{u}_x[\mathrm{O_2}])\right)+h[\mathrm{O_2}]\frac{\partial}{\partial t}(\ {}^{i}\mathrm{X})=\cdots$$

$$+h\frac{\partial}{\partial x}\left(\kappa_x\frac{\partial\left([\mathrm{O_2}]\ {}^{i}\mathrm{X}\right)}{\partial x}\right)+h\frac{\partial}{\partial x}\left(\mathrm{u}_x[\mathrm{O_2}]\ {}^{i}\mathrm{X}\right)$$

3b. $\left(\ldots + h\frac{\partial}{\partial x}\left(\kappa_x \frac{\partial[O_2]}{\partial x}\right) + h\frac{\partial}{\partial x}(u_x[O_2])\right) + h[O_2]\frac{\partial}{\partial t}\left({}^{i}X\right)\frac{1}{{}^{i}X} = \cdots$

$$+h\frac{\partial}{\partial x}\left(\kappa_x \frac{\partial\left([O_2]\ {}^{i}X\right)}{\partial x}\right)\frac{1}{{}^{i}X} + h\frac{\partial}{\partial x}\left(u_x[O_2]\ {}^{i}X\right)\frac{1}{{}^{i}X}$$

3c. $h[O_2]\frac{\partial}{\partial t}\left({}^{i}X\right)\frac{1}{{}^{i}X} = \cdots$

$$+h\frac{\partial}{\partial x}\left(\kappa_x \frac{\partial\left([O_2]\ {}^{i}X\right)}{\partial x}\right)\frac{1}{{}^{i}X} - h\frac{\partial}{\partial x}\left(\kappa_x \frac{\partial[O_2]}{\partial x}\right) + h\frac{\partial}{\partial x}\left(u_x[O_2]\ {}^{i}X\right)\frac{1}{{}^{i}X} - h\frac{\partial}{\partial x}(u_x[O_2])$$

4. $h[O_2]\frac{\partial {}^{17}\Delta}{\partial t} = \cdots$

$$+h\left(\frac{\partial}{\partial x}\left(\kappa_x \frac{\partial\left([O_2]^{17}X\right)}{\partial x}\right)\frac{1}{{}^{17}X} - \lambda\frac{\partial}{\partial x}\left(\kappa_x \frac{\partial\left([O_2]^{18}X\right)}{\partial x}\right)\frac{1}{{}^{18}X}\right) - h(1-\lambda)\left(\frac{\partial}{\partial x}\left(\kappa_x \frac{\partial[O_2]}{\partial x}\right)\right)$$

$$+h\left(\frac{\partial\left(u_x[O_2]^{17}X\right)}{\partial x}\frac{1}{{}^{17}X} - \lambda\frac{\partial\left(u_x[O_2]^{18}X\right)}{\partial x}\frac{1}{{}^{18}X}\right) - h(1-\lambda)\left(\frac{\partial(u_x[O_2])}{\partial x}\right)$$

Light-dependent processes

1. $\frac{\partial}{\partial t}(h[O_2]) = \cdots - \mathrm{LD}$

2. $\frac{\partial}{\partial t}\left(h[O_2]\ {}^{i}X\right) = \cdots - \mathrm{LD}\ {}^{i}X\ {}^{i}\alpha_{k,LD}$

3. $h[O_2]\frac{\partial}{\partial t}\left({}^{i}X\right)\frac{1}{{}^{i}X} = \cdots - \mathrm{LD}\left({}^{i}\alpha_{k,LD} - 1\right)$

4a. $h[O_2]\frac{\partial {}^{17}\Delta}{\partial t} = \cdots - \mathrm{LD}\left(\left({}^{17}\alpha_{k,LD} - 1\right) - \lambda\left({}^{18}\alpha_{k,LD} - 1\right)\right)$

Or, if the process consumes O_2 directly from photosynthetic production:

4b. $h[O_2]\frac{\partial {}^{17}\Delta}{\partial t} = \cdots - \mathrm{LD}\left(\left(\frac{{}^{17}X_w\,{}^{17}\alpha_{k,P}\,{}^{17}\alpha_{k,LD}}{{}^{17}X} - 1\right) - \lambda\left(\frac{{}^{18}X_w\,{}^{18}\alpha_{k,P}\,{}^{18}\alpha_{k,LD}}{{}^{18}X} - 1\right)\right)$

Bubble processes

Bubble exchange and ebullition are solved analogously to air-water gas exchange. Bubble injection is the special case where ${}^{i}X_j = {}^{i}X_a$ and injected bubbles completely dissolve. With complete dissolution there cannot be net fractionation or loss of gas from the water column back into the bubble; thus the effective ${}^{i}\alpha_k = {}^{i}\alpha_k = 1$, $-F_{b,inj} = 0 \neq +F_{b,inj}$, and the resulting equation for bubble injection has no terms dependent on $[O_2]$ and is dependent only on the bubble injection flux.

Example calculation

An example calculation of hourly GOP_{TOI} using the data from 7/29/2014 10:00 and 12:04, using Equations 3a through 3c in the main text (change in tracer with time, production, and air-water gas exchange).

Change in tracer with time

h=0.25 m

t_1=10:00; t_2=12:04; ∂t=2.067 h

$[O_2]$=206.2 μmol kg^{-1} (average over t_1 to t_2 at sonde location)

$^{17}\Delta_1$=89.2 per meg; $^{17}\Delta_1$=121.6 per meg; $\partial^{17}\Delta$=32.4 per meg=3.24×10^{-5} (at sample location)

$$h[O_2]\frac{\partial}{\partial t}\left(^{17}\Delta\right) = \frac{(0.25)(206.2)\left(3.24\times10^{-5}\right)}{2.067} = \ 8.08\times10^{-4}\ \mu mol\ kg^{-1}\ \ O_2\ m\ h^{-1}$$

Air-water gas exchange

k_{O2} =6.80 cm h^{-1}=0.0680 m h^{-1}

$[O_2]_{sat}$=222.0 mmol m^{-3} (average at sonde location)

$^{18}\alpha_e$=1.00071; $^{17}\alpha_e$=1.00038 (average at sonde location)

$^{18}\alpha_k$=0.9978; $^{17}\alpha_k=0.9978^{0.517}$=0.9989

$^{18}X_a$=1;$^{17}X_a$=1

$^{18}X=(^{18}\delta/1000-1)$=-6.6206/1000+1=0.99338; ^{17}X=-3.3293/1000+1=0.99667 (average at sample location)

$^{18}A_G=(^{18}\alpha_e\,^{18}\alpha_k\,^{18}X_a/^{17}X)-1$=(1.00071)(0.9978)(1)/(0.99338)-1=0.005165; $^{17}A_G$=0.002576

λ=0.5179

$$k_{O2}[O_2]_{sat}\left(^{17}A_G - \lambda\,^{18}A_G\right) - \ k_{O2}[O_2]\left(\left(^{17}\alpha_k - 1\right) - \lambda\left(^{18}\alpha_k - 1\right)\right)=$$

(0.0680)(222.0)(0.002576-0.5179[0.005165])-(6.80)(206.2)([0.9989-1]-0.5179[0.9978-1])=

-15.05×10^{-4} μmol kg^{-1} O_2 m h^{-1}

Production

$^{18}\alpha_P$=1.00397; $^{17}\alpha_P$=1.00214 (average at sonde location, calculated as in Manning et al. 2017 but excluding coccolithophores)

$^{18}X_W$=0.97503;$^{17}X_W$=0.98724 average at sonde location, calculated as in Manning et al. 2017)

$^{18}A_P=(^{18}\alpha_P\,^{18}X_W/^{17}X)-1$=(1.00397)(0.97515)/(0.99338)-1=-0.014452; $^{17}A_P$=-0.007347

$GOP\left(^{17}A_P - \lambda\,^{18}A_P\right)$=(-0.007347-0.5179[-0.014452ans)=GOP(117.38×10^{-4} μmol kg^{-1} O_2 m h^{-1})

Solve for GOP

$$h[O_2]\frac{\partial}{\partial t}\left({}^{17}\Delta\right) = \mathrm{GOP}\left({}^{17}A_P - \lambda^{18}A_P\right)$$

$$+ k_{O2}[O_2]_{sat}\left({}^{17}A_G - \lambda^{18}A_G\right) - k_{O2}[O_2]\left(\left({}^{17}\alpha_k - 1\right) - \lambda\left({}^{18}\alpha_k - 1\right)\right)$$

$$\mathrm{GOP} = \left[h[O_2]\frac{\partial}{\partial t}\left({}^{17}\Delta\right) - (k_{O2}[O_2]_{sat}\left({}^{17}A_G - \lambda^{18}A_G\right) - k_{O2}[O_2]\left(\left({}^{17}\alpha_k - 1\right) - \lambda\left({}^{18}\alpha_k - 1\right)\right))\right] /$$

$$\left({}^{17}A_P - \lambda^{18}A_P\right)$$

$=(8.08\times10^{-4} - (-15.05\times10^{-4})/(1.38\times10^{-4}) = 16.8$ μmol kg^{-1} O_2 m h^{-1}

GOP (ρ)= 16.8 μmol kg^{-1} O_2 m h^{-1} (1.012 kg m^{-3})(mmol/1000 μmol)=17.0 mmol O_2 m^{-2} h^{-1}

(check value for 11:00, Figure 2a)

References

Angert, A., S. Rachmilevitch, E. Barkan, and B. Luz. 2003. Effects of photorespiration, the cytochrome pathway, and the alternative pathway on the triple isotopic composition of atmospheric O_2. *Glob. Biogeochem. Cycles* 17(1): 1030. doi: 0.1029/2002GB00193

Bender, M., J. Orchardo, M-L. Dickson, R. Barber, and S. Lindley. 1999. In vitro O_2 fluxes compared with ^{14}C production and other rate terms during the JGOFS Equatorial Pacific experiment. *Deep Sea Res I* 46(4): 637-654. doi: 10.1016/S0967-0637(98)00080-6.

Benson, B.B., and D. Krause Jr. 1980. The concentration and isotopic fractionation of gases dissolved in freshwater in equilibrium with the atmosphere: 1. Oxygen. *Limnol. Oceanogr.* 25(4): 662-671. doi: 10.4319/lo.1980.25.4.0662

Benson, B.B., and D. Krause Jr. 1984. The concentration and isotopic fractionation of oxygen dissolved in freshwater and seawater in equilibrium with the atmosphere. *Limnol. Oceanogr.* 29(3): 620-632. doi: 10.4319/lo.1984.29.3.0620Eisenstadt

Garcia, H.E., and L.I. Gordon. 1992. Oxygen solubility in seawater: Better fitting equations. *Limnol. Oceanogr.* 37(6): 1307-1312. doi: 10.4319/lo.1992.37.6.1307

Garcia, H.E., and L.I. Gordon. 1993. Erratum: Oxygen solubility in seawater: Better fitting equations. *Limnol. Oceanogr.* 38(3): 656. doi: 10.4319/lo.1993.38.3.0643

Hamme, R.C., N. Cassar, V.P. Lance, R.D. Vaillancourt, M.L. Bender, P.G. Strutton, T.S. Moore, M.D. DeGrandpre, C.L. Sabine, D.T. Ho, and B.R. Hargreaves. 2012. Dissolved O_2/Ar and other methods reveal rapid changes in productivity during a Lagrangian experiment in the Southern Ocean. *J. Geophys. Res. Oceans* 117(C00F12): 1-19. doi: 10.1029/2011JC007046.

Helman, Y., E. Barkan, D. Eisenstadt, and A. Kaplan. 2005. Fractionation of the three stable oxygen isotopes by oxygen-proucing and oxygen-consuming reactions in photosynthetic organisms. *Plant Physiol.* 138(4): 2292-2298. doi: 10.1104/pp.105.063768

Howard, E.M., C.A. Durkin, G.M.M. Hennon, F. Ribalet, R.H.R. Stanley. Biological production, export efficiency, and phytoplankton communities across 8000 km of the South Atlantic. *Glob. Biogeochem. Cycles* 31(7): 1066-1088. doi: 10.1002/2016GB005488

Kaiser, J. 2011. Technical note: Consistent calculation of aquatic gross production from oxygen triple isotope measurements. *Biogeosci*. 8(7): 1793-1811. doi: 10.5194/bg-8-1793-2011

Kana, T.M. 1990. Light-dependent oxygen cycling measured by an oxygen-18 isotope dilution method. *Mar. Ecol. Prog. Ser.* 64(3): 293-300. doi: 10.3354/meps064293

Li, B., L.Y. Yeung, H. Hu, and J.L. Ash. 2019. Kinetic and equilibrium fractionation of O_2 isotopologues during air-water gas transfer and implications for tracing oxygen cycling in the ocean. *Mar. Chem.* 210: 61-71. doi: 10.1016/j.marchem.2019.02.006

Luz, B., and E. Barkan. 2005. The isotopic ratios $^{17}O/^{16}O$ and $^{18}O/^{16}O$ in molecular oxygen and their significance in biogeochemistry. *Geochimica et Cosmochimica Acta* 69(5): 1099-1110. doi: 10.1016/j.gca.2004.09.001

Luz, B., and E. Barkan. 2011. Proper estimation of marine gross O^2 production with $^{17}O/^{16}O$ and 18O/16O ratios of dissolved O_2. *Geophys. Res. Lett.* 38(19): L19606. doi:10.1029/2011GL049138

Manning, C.C., E.M. Howard, D.P. Nicholson, B.Y. Ji, Z.O. Sandwith, and R.H.R. Stanley. 2017, Revising estimates of aquatic gross oxygen production by the triple oxygen isotope method to incorporate the local isotopic composition of water. *Geophys. Res. Lett.* 44(20): 10511-10519. doi: 10.1002/2017GL074375

Nicholson, D., R.H.R. Stanley, and S.C. Doney. The triple oxygen isotope tracer of primary productivity in a dynamic ocean model. *Glob. Biogeochem. Cycles* 28(5): 538-552. doi: 10.1002/2013GB004704

Prokopenko, M.G., O.M. Pauluis, J. Granger, and L.Y. Yeung. 2011. Exact evaluation of gross photosynthetic production from the oxygen triple-isotope composition of O_2: Implications for the net-to-gross primary production ratios. *Geophys, Res. Lett.* 38(14): L14603. doi: 10.1029/2011GL047652

Vachon, D., and Y.T. Prairie. 2013. The ecosystem size and shape dependence of gas transfer velocity versus wind speed relationships in lakes. *Canadian J. Fish. Aquat. Sci.* 70(12): 1757-1764. doi: 10.1139/cjfas-2013-0241

Dissolved oxygen and triple oxygen isotope measurements provide different insights into gross oxygen productio
Estuaries and Coasts

Evan M. Howard*, Amanda C. Spivak, Jennifer S. Karolewski, Kelsey M. Gosselin, Zoe O. Sandwith, Cara C. Ma
*Corresponding author: ehoward2@uw.edu, School of Oceanography, University of Washington, Seattle, WA, U

Supporting tables, including:

Table S1. Triple oxygen isotope ratios and concurrently sampled environmental variables

Table S2. Spatial surveys of oxygen saturation state and effect sizes across study

Table S3. Correlations of productivity and environmental variables

ı in a shallow salt marsh por

anning, Rachel H. R. Stanley
S/

Table S1. Triple oxygen isotope ratios and concurrently sampled environmental variables
Triple oxygen isotope ratios, as well as colocated measurements of temperature, dissolved oxygen saturation state (O_2 sat. state), and salinity (measured via refractometer, and reported as absolute salinity). Additionally, triple oxygen isotope ratios from air-equilibrated water standards from both the standard and low-O_2 analytical methods used in this study.

Environmental samples

Date	Time	Location	Temperature	O_2 sat. state	Salinity	$^{17}\Delta$	$\delta^{18}O$	$\delta^{17}O$	$\delta^{17}O$ recalculated from	Notes
dd/mm/yyyy	hh:mm		(°C)	(%)	(g/kg)	(per meg)	(per mil)	(per mil)	$^{17}\Delta$ and $\delta^{18}O$ (per mil)	
5/21/2014	9:51		2	18.1	90.8	26.5	84	-4.54	-2.27	-2.27	
5/21/2014	9:51		2	18.1	90.8	26.5	85	-4.95	-2.48	-2.48	
5/21/2014	12:00		2	21.5	127.7	26.5	114	-7.74	-3.91	-3.90	
5/21/2014	12:00		2	21.5	127.7	26.5	122	-7.98	-4.03	-4.02	
5/21/2014	12:00		2	21.5	127.7	26.5	118	-7.90	-3.99	-3.98	
5/21/2014	13:56		3	24.1	128.2	26.5	112	-7.56	-3.82	-3.81	
5/21/2014	13:56		3	24.1	128.2	26.5	105	-7.35	-3.72	-3.71	
5/29/2014	10:25		3	13.8	106.2	26.0	69	-6.12	-3.11	-3.10	
5/29/2014	12:01		2	17.0	121.1	26.0	64	-5.45	-2.77	-2.76	
5/29/2014	14:03		2	19.7	134.1	26.0	51	-5.35	-2.73	-2.72	
5/29/2014	10:25		3	13.8	106.2	26.0	94	0.64	0.43	0.43	at shore
5/29/2014	11:58		2	16.8	121.1	26.0	84	1.04	0.62	0.62	at shore
5/29/2014	14:03		2	19.7	134.1	26.0	80	1.33	0.77	0.77	at shore
5/29/2014	10:17		1	13.6	96.9	26.0	73	1.74	0.98	0.98	
5/29/2014	12:10		1				76	2.00	1.11	1.11	
5/29/2014	9:58		5	12.9	107.9	27.5	86	2.80	1.54	1.54	
5/29/2014	12:21		5				121	3.81	2.09	2.09	
5/29/2014	12:13		8				116	3.43	1.89	1.89	~ 5-10 cm bottom depth
5/29/2014	12:17		3				67	3.11	1.68	1.68	
5/29/2014	12:19		4				76	3.06	1.66	1.66	
6/11/2014	9:53		3	20.1	110.7	28.0	121	-8.73	-4.42	-4.41	
6/11/2014	11:53		3	22.8	139.2	28.0	132	-9.71	-4.92	-4.91	
6/11/2014	11:53		3	22.8	139.2	28.0	140	-9.86	-4.99	-4.98	
6/11/2014	13:53		2	25.1	150.5	28.0	140	-9.32	-4.71	-4.70	
6/19/2014	10:25		4	23.4	80.4	30.0	91	-6.72	-3.40	-3.40	
6/19/2014	11:57		4	25.6	111.2	30.0	115	-7.84	-3.96	-3.95	
6/19/2014	13:57		4	27.6	132.8	30.0	120	-8.33	-4.21	-4.20	
6/24/2014	9:56		7	22.0	93.0	31.0	115	-7.88	-3.98	-3.97	
6/24/2014	11:58		7	25.6	123.6	31.0	104	-7.74	-3.92	-3.91	
6/24/2014	13:52		7	27.5	162.0	31.0	127	-8.15	-4.11	-4.11	
6/24/2014	10:06		2	21.9	76.2	31.0	125	-8.93	-4.52	-4.51	
6/24/2014	12:08		2	24.6	104.6	31.0	76	-5.02	-2.53	-2.53	
6/24/2014	14:02		2	27.0	121.3	31.0	86	-5.76	-2.91	-2.90	
6/30/2014	11:04	Between 3 and 4		26.8	95.9	31.5	89	-5.74	-2.89	-2.89	
6/30/2014	12:13	Between 3 and 4		28.1	106.0	31.5	116	-6.86	-3.45	-3.44	Tube[a] 3 m offshore, over macroalgae
6/30/2014	12:15	Between 3 and 4		28.1	106.0	31.5	131	-7.64	-3.84	-3.84	Tube[a] 3 m offshore, over macroalgae
6/30/2014	13:17	Between 3 and 4		28.3	123.4	31.5	127	-7.68	-3.86	-3.86	Tube[a] 3 m offshore, over macroalgae
6/30/2014	11:15	Between 3 and 4		26.9	87.3	31.5	135	-8.16	-4.11	-4.10	Tube[a] 3 m offshore, over macroalgae
6/30/2014	12:29	Between 3 and 4		27.6	111.9	31.5	111	-6.40	-3.21	-3.21	Tube[a] 3 m offshore, over microalgae
6/30/2014	13:32	Between 3 and 4		29.2	125.8	31.5	152	-8.28	-4.16	-4.15	Tube[a] 3 m offshore, over microalgae
7/8/2014	11:31	Between 1 and 7		29.9	113.6	27.0	136	-8.44	-4.26	-4.25	Tube[a] 3 m offshore, over microalgae
7/8/2014	12:35	Between 1 and 7		30.0	120.4	27.0	111	-8.44	-4.28	-4.27	Tube[a] 3 m offshore, over microalgae
7/8/2014	13:56	Between 1 and 7		30.6	124.2	27.0	121	-7.77	-3.92	-3.91	Tube[a] 3 m offshore, over microalgae
7/8/2014	11:18	Between 1 and 7		29.9	131.6	27.0	118	-7.23	-3.64	-3.63	Tube[a] 3 m offshore, over microalgae
7/8/2014	12:36	Between 1 and 7		30.2	144.1	27.0	150	-10.29	-5.20	-5.19	Tube[a] 3 m offshore, over macroalgae
7/8/2014	13:51	Between 1 and 7		29.5	155.9	27.0	147	-9.95	-5.03	-5.02	Tube[a] 3 m offshore, over macroalgae
7/8/2014	14:21	Between 1 and 7		29.5	155.9	27.0	140	-9.69	-4.90	-4.89	Tube[a] 3 m offshore, over macroalgae
7/10/2014	9:53		4	24.4	76.3	30.5	154	-9.77	-4.93	-4.92	Tube[a] 3 m offshore, over macroalgae
7/10/2014	11:50		4	26.2	117.0	30.5	111	-8.09	-4.10	-4.09	
7/10/2014	11:50		4	26.2	117.0	30.5	141	-9.48	-4.79	-4.78	
7/10/2014	13:56		4	28.5	150.9	30.5	149	-9.61	-4.85	-4.84	
7/17/2014	10:08		4	21.9	97.9	31.0	149	-10.05	-5.08	-5.07	
7/17/2014	12:02		4	25.0	136.8	31.0	92	-6.36	-3.21	-3.21	
7/17/2014	14:01		4	27.2	171.4	31.0	150	-10.19	-5.16	-5.14	
7/17/2014	9:57		8	23.8	198.0	31.0	209	-14.28	-7.24	-7.21	
7/17/2014	11:48		8	28.8	251.1	31.0	192	-12.64	-6.39	-6.37	~ 5-10 cm bottom depth
7/17/2014	13:51		8	30.6	269.4	31.0	199	-12.71	-6.43	-6.41	~ 5-10 cm bottom depth
7/22/2014	11:16	Near 4		27.0	87.9	29.5	164	-11.31	-5.73	-5.71	~ 5-10 cm bottom depth
7/22/2014	12:14	Near 4		27.7	114.4	29.5	151	-11.32	-5.75	-5.73	Tube[a] 3 m offshore, over macroalgae
7/22/2014	13:24	Near 4		29.3	126.2	29.5	183	-11.45	-5.78	-5.76	Tube[a] 3 m offshore, over macroalgae
7/22/2014	13:26	Near 4		29.3	126.2	29.5	132	-10.50	-5.34	-5.32	Tube[a] 3 m offshore, over macroalgae
7/22/2014	11:18	Near 4		27.4	85.6	29.5	128	-10.62	-5.40	-5.39	Tube[a] 3 m offshore, over macroalgae
7/22/2014	12:17	Near 4		26.3	106.5	29.5	132	-10.72	-5.45	-5.43	Tube[a] 3 m offshore, over microalgae
7/22/2014	13:23	Near 4		29.4	116.6	29.5	122	-10.45	-5.32	-5.30	Tube[a] 3 m offshore, over microalgae
7/23/2014	10:02		1	26.8	87.5	31.5	153	-10.00	-5.05	-5.04	Tube[a] 3 m offshore, over microalgae
7/23/2014	11:51		1	29.5	122.8	31.5	129	-7.13	-3.57	-3.57	
7/23/2014	11:51		1	29.5	122.8	31.5	133	-8.25	-4.16	-4.15	
7/23/2014	13:55		1	32.2	140.2	31.5	101	-8.29	-4.21	-4.20	
7/29/2014	5:59		1	20.0	33.7	29.5	118	-7.88	-3.98	-3.97	
7/29/2014	6:31		1	19.9	36.4	29.5	52	2.75	1.48	1.48	
7/29/2014	7:33		1	20.1	49.8	29.5	42	1.52	0.83	0.83	
7/29/2014	8:31		1	20.8	66.1	29.5	74	-3.01	-1.49	-1.49	
7/29/2014	10:00		1	22.5	89.7	29.5	82	-4.08	-2.04	-2.03	
7/29/2014	12:04		1	25.1	115.3	29.5	89	-5.99	-3.02	-3.02	
7/29/2014	13:59		1	27.8	134.8	29.5	122	-7.23	-3.64	-3.63	
7/29/2014	15:33		1	28.6	134.3	29.5	140	-7.82	-3.92	-3.92	
7/29/2014	16:58		1	27.9	116.5	29.5	148	-7.64	-3.83	-3.82	
7/29/2014	18:01		1	26.6	96.5	29.5	133	-6.54	-3.27	-3.26	
7/29/2014	18:41		1	26.1	88.2	29.5	115	-4.59	-2.27	-2.27	
8/7/2014	9:58		4	21.9	84.9	29.0	96	-3.70	-1.82	-1.82	
8/7/2014	10:59		4	22.8	104.6	29.0	93	-6.66	-3.37	-3.36	
8/7/2014	12:01		4	24.0	128.1	29.0	121	-7.41	-3.73	-3.72	
8/7/2014	12:57		4	25.2	149.8	29.0	133	-8.59	-4.34	-4.33	
8/7/2014	14:00		4	26.8	175.0	29.0	78	-9.15	-4.68	-4.67	
8/19/2014	9:56		4	20.9	78.8	31.0	155	-10.03	-5.06	-5.05	
8/19/2014	10:57		4	22.7	97.9	31.0	146	-10.36	-5.25	-5.24	
8/19/2014	11:57		4	24.0	135.7	31.0	164	-11.21	-5.68	-5.66	
8/19/2014	13:57		4	26.5	154.8	31.0	175	-11.81	-5.98	-5.96	
8/26/2014	9:10		4	23.8	58.3	32.0	175	-10.67	-5.38	-5.37	
8/26/2014	9:59		4	25.4	79.1	32.0	129	-8.56	-4.32	-4.31	
8/26/2014	10:57		4	27.0	90.2	32.0	145	-9.14	-4.61	-4.60	
8/26/2014	12:01		4	29.0	109.5	32.0	169	-9.72	-4.89	-4.88	
8/26/2014	13:02		4	30.0	132.1	32.0	160	-9.57	-4.82	-4.81	
8/26/2014	14:02		4	30.9	130.2	32.0	166	-9.56	-4.81	-4.80	
8/26/2014	15:03		4	31.2	132.2	32.0	147	-8.48	-4.26	-4.25	
8/26/2014	16:03		4	31.1	130.4	32.0	142	-7.38	-3.69	-3.69	
8/26/2014	9:24	Sensor location					148	-6.80	-3.39	-3.38	
							142	-7.43	-3.72	-3.71	

8/26/2014	10:20	Sensor location				133	-8.76	-4.42	-4.41
8/26/2014	11:33	Sensor location				165	-9.96	-5.02	-5.01
8/26/2014	12:18	Sensor location				166	-10.13	-5.10	-5.09
8/26/2014	13:21	Sensor location				165	-9.63	-4.85	-4.84
8/26/2014	14:19	Sensor location				168	-9.10	-4.57	-4.56
9/3/2014	10:01	4	24.0	95.0	34.5	104	-6.71	-3.38	-3.38 Potential salinity error[b]
9/3/2014	12:00	4	26.8	145.9	34.5	140	-8.32	-4.18	-4.18 Potential salinity error[b]
9/3/2014	13:00	4	27.9	161.2	34.5	149	-8.72	-4.39	-4.38 Potential salinity error[b]
9/3/2014	13:51	4	28.3	167.7	34.5	146	-8.93	-4.50	-4.49 Potential salinity error[b]
9/17/2014	10:02	4	16.4	64.6	31.5	108	-6.40	-3.22	-3.21 Potential salinity error[b]
9/17/2014	10:59	4	18.0	96.0	31.5	136	-9.43	-4.77	-4.76 O_2 precision 0.4%, not 0.2%
9/17/2014	11:01	4	18.1	96.0	31.5	141	-9.57	-4.84	-4.83 O_2 precision 0.4%, not 0.2%
9/17/2014	11:03	4	18.2	96.0	31.5	132	-9.03	-4.57	-4.56 O_2 precision 0.4%, not 0.2%
9/17/2014	11:05	4	18.3	96.0	31.5	135	-9.18	-4.64	-4.63 O_2 precision 0.4%, not 0.2%
9/17/2014	11:07	4	18.4	96.0	31.5	129	-9.34	-4.73	-4.72 O_2 precision 0.4%, not 0.2%
9/17/2014	12:00	4	19.5	121.7	31.5	149	-9.91	-5.01	-5.00 O_2 precision 0.6%, not 0.2%
9/17/2014	13:02	4	20.9	128.6	31.5	144	-10.00	-5.06	-5.05 O_2 precision 0.4%, not 0.2%
9/17/2014	14:00	4	21.8	145.0	31.5	158	-10.03	-5.06	-5.05 O_2 precision 0.4%, not 0.2%
9/23/2014	10:02	1	14.9	61.6	35.0	89	-3.92	-1.95	-1.94 Potential salinity error[b]
9/23/2014	11:01	1	16.1	74.3	35.0	74	-4.85	-2.45	-2.44 Potential salinity error[b]
9/23/2014	12:02	1	17.9	87.9	35.0	93	-5.44	-2.73	-2.73 Potential salinity error[b]
9/23/2014	13:01	1	19.6	102.5	35.0	114	-6.19	-3.10	-3.10 Potential salinity error[b]
9/23/2014	14:08	1	20.8	112.7	35.0	113	-5.85	-2.92	-2.92 Potential salinity error[b]
9/30/2014	9:59	4	14.7	76.3	36.5	24	-1.20	-0.60	-0.60 Potential salinity error[b]
9/30/2014	11:00	4	15.1	92.5	36.5	57	-3.72	-1.87	-1.87 Potential salinity error[b]
9/30/2014	11:58	4	15.1	100.4	36.5	68	-4.76	-2.40	-2.40 Potential salinity error[b]
9/30/2014	12:59	4	15.4	106.9	36.5	81	-5.42	-2.74	-2.73 Potential salinity error[b]
9/30/2014	12:59	4	15.4	106.9	36.5	80	-5.57	-2.81	-2.81 Potential salinity error[b]
9/30/2014	13:54	4	15.4	114.1	36.5	87	-5.88	-2.97	-2.96 Potential salinity error[b]
10/14/2014	10:02	1	15.1	73.7	32.5	49	-2.70	-1.35	-1.35
10/14/2014	11:04	1	16.2	80.0	32.5	65	-3.53	-1.76	-1.76
10/14/2014	12:02	1	17.8	90.3	32.5	83	-4.34	-2.17	-2.17
10/14/2014	12:02	1	17.8	90.3	32.5	84	-4.39	-2.19	-2.19
10/14/2014	13:02	1	18.5	98.7	32.5	83	-4.61	-2.31	-2.31
10/14/2014	14:00	1	19.4	106.3	32.5	82	-4.65	-2.33	-2.33

[a] These samples were collected through 5 m lengths of Tygon tubing as environmental controls for benthic chamber experiements confucted concurrently with this work. Water was sampled at 10 cm depth over sediments with macroalgal cover, or sediments with only microalgae visible. Rates from these samples covered roughly 90 minutes, and thus are not used to calculate daily production rates, but are included in the comparison of hourly GOP rates.

[b] The handheld refractometer used to determine salinity developed condensation between the prism and sample plate on these days, which may have biased readings. Salinity calculated from sensor conductivity measurements was lower than from the refractometer during these periods.

Water standards

Date	Time	$^{17}\Delta$	$\delta^{18}O$	$\delta^{17}O$	$\delta^{17}O$ recalculated from $^{17}\Delta$ and $\delta^{18}O$ (per mil)	Notes
6/4/14	0:40	7	0.64	0.34	0.34	
7/4/14	2:16	11	0.68	0.36	0.36	
7/4/14	4:56	9	0.67	0.36	0.36	
7/4/14	10:17	15	0.37	0.21	0.21	
7/4/14	12:54	12	0.67	0.36	0.36	
7/4/14	15:33	6	0.67	0.35	0.35	
7/6/14	19:02	14	0.67	0.36	0.36	
7/7/14	10:06	1	0.66	0.35	0.35	
7/9/14	23:43	9	0.68	0.36	0.36	
7/12/14	18:47	19	0.67	0.37	0.37	
7/17/14	0:56	0	0.66	0.34	0.34	
7/17/14	11:35	-2	0.69	0.35	0.35	
7/19/14	9:49	13	0.69	0.37	0.37	
7/20/14	17:35	8	0.68	0.36	0.36	
7/23/14	22:10	14	0.69	0.37	0.37	
7/25/14	14:06	2	0.68	0.35	0.35	
7/26/14	5:58	6	0.69	0.36	0.36	
7/27/14	23:17	9	0.68	0.36	0.36	
7/30/14	2:47	21	0.69	0.38	0.38	
7/30/14	16:13	16	0.66	0.36	0.36	
9/19/14	18:44	10	0.64	0.34	0.34	
9/20/14	2:09	3	0.66	0.35	0.35	
9/20/14	4:36	3	0.67	0.35	0.35	
9/25/14	18:18	4	0.64	0.33	0.33	
9/25/14	20:47	10	0.63	0.34	0.34	
9/25/14	23:18	5	0.63	0.33	0.33	
9/27/14	2:32	0	0.64	0.33	0.33	
9/27/14	12:26	9	0.63	0.33	0.33	
9/29/14	12:00	12	0.60	0.32	0.32	
9/30/14	10:18	0	0.56	0.29	0.29	
9/30/14	20:32	12	0.62	0.33	0.33	
10/2/14	19:46	4	0.64	0.34	0.34	Low O_2 method
10/2/14	22:37	1	0.66	0.34	0.34	Low O_2 method
10/6/14	17:40	20	0.63	0.35	0.35	Low O_2 method
10/6/14	20:40	8	0.62	0.33	0.33	Low O_2 method
10/9/14	12:19	15	0.64	0.34	0.34	Low O_2 method
10/13/14	14:35	20	0.64	0.35	0.35	Low O_2 method
10/14/14	14:11	4	0.64	0.34	0.34	Low O_2 method
10/28/14	16:17	5	0.68	0.36	0.36	Low O_2 method
10/28/14	19:08	7	0.68	0.36	0.36	Low O_2 method
10/31/14	15:50	7	0.68	0.36	0.36	Low O_2 method
11/4/14	13:01	5	0.71	0.37	0.37	Low O_2 method
11/13/14	7:37	9	0.59	0.31	0.31	
11/13/14	10:10	13	0.60	0.32	0.32	
11/15/14	8:41	13	0.57	0.31	0.31	
11/17/14	8:33	10	0.60	0.32	0.32	
11/18/14	19:41	12	0.58	0.31	0.31	
Mean(s.d.)		9(6)	0.64(0.05)	0.34(0.03)	0.34(0.03)	
CV		0.65	0.08	0.08	0.08	

Table S2. Spatial surveys of oxygen saturation state and effect sizes across study

Dissolved oxygen saturation state (O_2 sat. state) in morning and afternoon from spatial surveys of the study pond. Additionally, the mean, standard deviation (s.d.), and coefficient of variation (CV) across all surveys are summarized. Effect sizes of the rates of daily saturation state increases are calculated in terms of magnitude and variability, as the time-mean (or time-standard deviation) value at a sample location, normalized to the time-average across the pond (e.g. of the time-means (or standard deviation, s.d., in time) for each station. For example, for n station locations: effect size=$mean_{i(t\ initial\ to\ t\ final)}/Mean(mean_i,...,mean_n)$ or $s.d._{i(t\ initial\ to\ tf\ inal)}/Mean(s.d._i,...,s.d._n)$

Survey data

Date	Location	Time 1 (hh:mm)	O_2 sat. state (%)	Time 2 (hh:mm)	O_2 sat. state (%)	d/dt (O_2 sat. state) (% h^{-1})
5/29/2014	1	11:04	107.0	13:20	150.6	19.2
	2	11:04	109.1	13:29	136.0	11.1
	3	11:05	128.2	13:27	140.4	5.2
	4	10:58	150.2	13:26	179.7	12.0
	5	11:00	123.1	13:12	131.2	3.7
	6	11:12	134.8	13:21	174.9	18.7
	7	11:15	135.1	13:18	178.7	21.3
	8	11:17	171.1	13:15	209.5	19.5
7/17/2014	1	10:28	101.3	14:08	146.8	12.4
	2	10:33	91.9	14:06	117.6	7.2
	3	10:34	94.2	14:05	139.2	12.8
	4	10:36	110.1	14:15	175.5	17.9
	5	10:37	128.4	14:14	156.6	7.8
	6	10:31	230.6	14:07	343.8	31.4
	7	10:27	119.2	14:10	203.5	22.7
	8	10:25	191.8	14:11	253.4	16.4
7/23/2014	1	10:23	97.8	13:36	142.1	13.8
	2	10:21	81.8	13:34	117.6	11.1
	3	10:20	89.4	13:33	118.2	9.0
	4	10:19	92.8	13:32	136.9	13.7
	5	10:17	103.5	13:31	162.2	18.2
	6	10:24	183.1	13:37	287.2	32.4
	7	10:26	155.1	13:39	196.9	13.0
	8	10:28	207.6	13:40	231.2	7.4
8/7/2014	1	10:17	90.7	12:27	134.6	20.3
	2	10:20	78.1	12:30	114.4	16.8
	3	10:21	83.4	12:31	119.3	16.6
	4	10:22	94.0	12:32	144.0	23.1
	5	10:24	105.2	12:34	166.0	28.1
	6	10:18	169.9	12:28	257.2	40.3
	7	10:15	139.5	12:25	163.3	11.0
	8	10:13	184.2	12:23	228.1	20.3
9/23/2014	1	10:25	68.7	13:54	114.3	13.1
	2	10:23	64.2	13:52	108.4	12.7
	3	10:21	66.9	13:52	107.8	11.6
	4	10:20	67.0	13:51	112.7	13.0
	5	10:17	83.4	13:49	129.7	13.1
	6	10:26	112.9	13:55	190.3	22.2
	7	10:28	124.2	13:57	187.6	18.2
	8	10:29	114.4	13:58	202.2	25.2
10/13/2014	1	10:23	80.1	13:20	107.0	9.1
	2	10:21	72.7	13:19	100.3	9.3
	3	10:19	72.0	13:18	99.9	9.4
	4	10:17	72.5	13:17	100.9	9.5
	5	10:15	72.1	13:15	110.0	12.6
	6	10:24	81.4	13:21	170.4	30.2
	7	10:26	98.5	13:23	127.7	9.9
	8	10:28	86.1	13:25	166.5	27.3

Summary statistics			Effect sizes	
Location	Mean(s.d.)	CV	Magnitude	Variability
1	15 (4)	0.29	0.90	0.76
2	11 (3)	0.28	0.70	0.57
3	11 (4)	0.36	0.66	0.69
4	15 (5)	0.33	0.91	0.87
5	14 (9)	0.61	0.86	1.51
6	29 (8)	0.26	1.80	1.37
7	16 (5)	0.34	0.98	0.97
8	19 (7)	0.37	1.19	1.26

Table S3. Correlations of productivity and environmental variables

Cross-correlation coefficients (r, for Model II regression) and p values (for null hypothesis of no correlation) between anomalies in standardized daily rates ([x-mean(x)]/[standard deviation(x)]). Rates include: Gross primary production calculated from triple oxygen isotope ratios (GOP_{TOI}) and O_2 concentrations (GOP_{O2}), and nighttime respiration and sediment oxygen uptake (R), on prewhitened anomalies of environmental variables including temperature (T), photosynthetically active radiation flux (PAR), windspeed at 10 m (U_{10}), wind direction (U_{dir}), and the occurrence of recent flooding (within the previous day). ARIMA coefficients used in prewhitening are listed as (p, d, q) below each variable, and significant p values for correlations are identified using the shading scale below the table. The proportion of variance in GOP_{O2} and R which may be explained from the just the significantly correlated environmental variables is listed below each metabolic rate.

r	GOP_{TOI}[a] –	GOP_{O2} (0,1,1)	R (0,1,1)	T (1,1,1)	PAR (1,0,1)	U_{10} (1,0,1)	U_{dir} (1,0,1)	Flooding[c] (1,0,0)x(0,1,1)$_{27}$
GOP_{TOI}[a]		**0.56**	**0.63**	0.24	0.13	-0.38	0.24	-0.32
GOP_{O2}	**0.56**		**0.79**[b]	0.05	**0.65**	**-0.14**	**0.19**	**-0.20**
R	**0.63**	**0.83**[b]		0.02	**0.43**	**-0.21**	0.09	**-0.20**
Σ(Variance)		0.51	0.27					
p								
GOP_{TOI}[a]		**3×10^{-2}**	**6×10^{-3}**	2×10^{-1}	3×10^{-1}	6×10^{-2}	2×10^{-1}	1×10^{-1}
GOP_{O2}	**1×10^{-2}**		**3×10^{-24}** [b]	3×10^{-1}	**8×10^{-17}**	**4×10^{-2}**	**9×10^{-3}**	**6×10^{-3}**
R	**6×10^{-2}**	**4×10^{-26}** [b]		4×10^{-1}	**2×10^{-8}**	**4×10^{-3}**	1×10^{-1}	**5×10^{-3}**
						p<0.05	p<0.01	p<0.001

[a] Correlations with GOP_{TOI} were calculated from standardized anomalies based on only the subset of data from days when GOP_{TOI} was sampled. Data was not prewhitened for any variables in this reduced subset because of the small sample size and discontinuous series—autocorrelations and partial-autocorrelations were not improved by autoregression or moving averages.

[b] GOP_{O2} is calculated using R, and thus expected to be highly cross-correlated. Correlations are slightly different depending on which rate was used as the basis for ARIMA prewhitening.

[c] The occurrence of recent flooding was prewhitened using a multiplicative (i.e. periodic) ARIMA with differencing over 27 day spring-neap cycles, with a moving average between periods as well as a non-periodic ARIMA autoregressive term.